Chinese Chemical Letters 35 (2024) 108802

Contents lists available at ScienceDirect

Chinese Chemical Letters

journal homepage: www.elsevier.com/locate/cclet

Reducing the voltage loss of Y-series acceptor based organic solar cells *via* ternary/quaternary strategies

Pengyu Zhang, Zhiyang Zhang, Heng Sun, Jie Li, Yi Chen, Jiang Wang*, Chuanlang Zhan*

Key Laboratory of Advanced Materials Chemistry and Devices (AMC&DLab) of the Department of Education of Inner Mongolia Autonomous Region, Inner Mongolia Key Laboratory of Green Catalysis, College of Chemistry and Environment Science, Inner Mongolia Normal University, Huhehot 010022, China

ARTICLE INFO

Article history:
Received 18 April 2023
Revised 10 July 2023
Accepted 11 July 2023
Available online 14 July 2023

Keywords:
Organic solar cell
Ternary/quaternary strategy
Open-circuit voltage
Voltage loss
Non-radiative recombination loss

ABSTRACT

In recent years, with the emergence of non-fullerene fused-ring acceptors, power conversion efficiencies (PCEs) of organic solar cells (OSCs) have exceeded 19%. However, compared to inorganic or perovskite photovoltaic cells, a higher voltage loss has become one of the key factors limiting further improvement in the PCEs of OSCs. The ternary/quaternary strategy has been identified as a feasible and effective way to obtain high-efficiency OSCs. In this review, a brief outline is given of the key roles that guest materials played in reducing voltage losses in solar cell devices and a brief look at the future material design and the design of ternary/quaternary systems.

1. Introduction

Solution processable organic solar cells (OSCs) have attracted a lot of attention because of their low-cost, light-weight, mechanical-flexibility/stretchability, semi-transparency and roll-to-roll printing. With the efforts on design and synthesis of the electron donor/acceptor materials and device optimizations, the power conversion efficiencies (PCEs) of OSCs have rapidly increased to over 19% recently [1,2]. Typical polymer donor materials for use in fabricating high-performance OSCs include PBDB-T (poly[(2,6-(4,8-bis(5-(2-ethylhexyl)thiophen-2-yl)benzo[1,2-*b*:4,5-*b*]-dithiophene)-*co*-(1,3-di(5-thiophen-2-yl)-5,7-bis(2-ethylhexyl)benzo[1′,2′-*c*:4,5-*c*′] dithiophene-4,8–dione)]) and its halogenated derivatives, D18 (poly(dithieno[3,2-*e*:2′,3′-*g*]-2,1,3-benzothiadiazole-5,8-diyl(4-(2-butyloctyl)-2,5-thiophenediyl)(4,8-bis(5-(2-ethylhexyl)-4-fluoro-2-thienyl)benzo[1,2-*b*:4,5-*b*′]dithiophene-2,6-diyl)(3-(2-butyloctyl)-2,5-thiophenediyl))) and its chlorinated derivatives, and PTQ (poly(thiophene-quinoxaline) series [3–8]. Typical small-molecule donor materials include benzodithiophene terthiophene rhodanine (BTR) and its derivatives. For the past decade, non-fullerene acceptor materials have emerged one after another, which have pushed the rapid advances in the field of OSCs. In general, the nonfullerene small-molecule acceptors include the three main categories of fused-ring acceptor materials, such as the large ring class represented by PDI (perylene diimide) [9], the ITIC class (3,9-bis(2-methylene-(3-(1,1-dicyanomethylene)-indanone))-5,5,11,11-tetrakis(4-hexylphenyl)-dithieno[2,3-*d*:2′,3′-*d*′]-*s*-indaceno[1,2-*b*:5,6-*b*′]dithiophene) with IDT (indacenodithiophene) or IDTT (indacenodithieno[3,2-*b*]thiophene) or their analogs as the fused-ring cores [10] and the Y series with DA′D-type (D and A′ represent the electron-donating and accepting units, respectively) fused-ring structures as the centers [11]. With the structural modification of these three main types of acceptor materials, the PCEs have reached 10%, 15%, and more than 19%, respectively, the short-circuit current-density values (J_{SC}) have reached the levels of 18 mA/cm^2, 23 mA/cm^2, and 27 mA/cm^2, respectively, the fill-factors (FFs) have reached 67%, 77%, and 80%, respectively, and the open-circuit voltage (V_{OC}) values have reached approximately 0.80 V, 0.83 V and 0.87 V, respectively.

Organic semiconductor materials have narrow absorption bands, large exciton binding energies, and high recombination losses, relatively to inorganic semiconductors and perovskite materials. To further improve the device performance, by introducing a narrow-bandgap third component into the binary system, the solar spectral coverage of the active layer is extended and the absorption of the solar cell for near-infrared photons is increased, so that J_{SC} is increased. This strategy can improve FF by optimizing the structures of the guest components, but in order to obtain a low bandgap it is often necessary to reduce the LUMO energy levels of the guests, thus often leading to a decrease in V_{OC}. In contrast, the voltage-increased ternary strategy by increasing the LUMO energy level of the active layer acceptor phase to improve V_{OC} through

* Corresponding authors.
E-mail addresses: wangjiang@imnu.edu.cn (J. Wang), clzhan@imnu.edu.cn (C. Zhan).

https://doi.org/10.1016/j.cclet.2023.108802
1001-8417/

adding a guest acceptor component with a higher LUMO energy level has received much attention since it was proposed in 2019 [12–14]. By optimizing the structures of the D units in the centers of the A-D-A type acceptors, the structures of the end group A units and the side-chains, the strategies have developed a series of highly efficient ternary OSC material systems with ITIC-like and Y-series acceptors as the high-LUMO-level guest components, with efficiencies in the range of 15%–20%. Moreover, this strategy can also achieve V_{OC} enhancement by introducing a guest donor with a low HOMO energy level to lower the HOMO energy level of the donor phase [15,16]. In addition to the voltage-increased and current-increased ternary strategies, the device performance can be also improved by introducing a highly crystalline guest donor to form an alloy phase, by which increased FFs can be achieved [17–19].

To further improve the device performance of ternary OSCs, our group proposed a quaternary strategy in 2018 using PBDB-T: ITIC as the binary system and PCBM and ICBA as the third and fourth components. This strategy can synergistically enhance the light absorption, modulate the energy level alignment, and tune morphological properties, hence improve solar photons capturing and charge separation, transport and collection of the device by introducing two guest components. At the same time, the quaternary strategy can further improve the device performance by providing more material selectivity and mechanism selectivity by introducing one more guest component in comparison to the ternary strategy [20]. However, compared to the ternary strategy, the quaternary strategy increases the difficulty of design of the material system and the complexity of device optimization due to the use of four components [21]. Nevertheless, this strategy has been continuously explored as it can effectively improve the overall performance of the devices, and more than a dozen representative quaternary material systems have been developed, showing great competitiveness.

In this review, the research progress of ternary and quaternary OSCs based on the binary systems formed by high performance Y-series fused-ring acceptors for reducing device voltage losses is discussed. The intrinsic factors for reducing voltage losses and promoting the solar cell performance with ITIC-like and Y-series guest acceptors as well as with polymers and small molecules as guest donors are systematically described from the perspectives of both guest acceptors and guest donors by correlating the chemical structural characteristics of the guest components, providing material system design ideas for promoting the development of OSCs.

2. Voltage loss

With the emergence of the Y-series acceptors, the V_{OC}, J_{SC} and FF of OSCs have reached 0.85 V, 27 mA/cm^2 and 80% respectively, and the efficiencies have even reached beyond 19%. The development of OSCs is about to enter a new level of 20% efficiency. Although there is still a large area of improvement in J_{SC} and FF, the V_{OC} loss has become a key factor limiting further improvement in efficiency to a certain extent, and exploring strategies that can achieve J_{SC} and FF improvement while reducing voltage loss is beneficial to the further development of research. As shown in Fig. 1a, for any kinds of single-junction solar cells, the energy loss (E_{loss}) involves the following three parts (Eq. 1) [22].

$$\begin{aligned} E_{loss} &= E_g - qV_{OC} \\ &= \left(E_g - qV_{OC}^{SQ}\right) + \left(qV_{OC}^{SQ} - qV_{OC}^{rad}\right) + \left(qV_{OC}^{rad} - qV_{OC}\right) \\ &= \left(E_g - qV_{OC}^{SQ}\right) + q\Delta V_{OC}^{rad} + q\Delta V_{OC}^{non-rad} \\ &= \Delta E_1 + \Delta E_2 + \Delta E_3 \end{aligned} \quad (1)$$

where E_g is the optical bandgap of the blend film, q is the elementary charge, and V_{OC}^{SQ} is the maximum voltage obtained from the Shockley-Queisser (SQ) theory limit. ΔE_1, $(E_g - qV_{OC}^{SQ})$ is due to radiative recombination originating from the absorption above the gap, usually located at 0.25 eV or above, which is unavoidable for any single-junction solar cells. ΔE_2, $(q\Delta V_{OC}^{rad})$ is due to the additional radiative recombination from the absorption below the optical gap. For the best OSCs, whose values essentially lie around 0.05 eV, ΔE_2 is comparable to Si and GaAs-based solar cells. ΔE_2 is associated with the existence of charge transfer (CT) states, whose energy levels are located below the bandgap and whose absorption is located in the more redshifted region. By reducing the energetic disorder, it is beneficial to reduce or eliminate the CT state absorption and thus reduce the radiative energy loss below the bandgap. ΔE_3, $(q\Delta V_{OC}^{non-rad})$ arises from the non-radiative recombination, it can be calculated by the following equation (Eq. 2):

$$\Delta E_3 = qV_{OC}^{non-rad} = nkT\ln(EQE_{EL}) \quad (2)$$

where k is the Boltzmann constant and T is the temperature of the device; EQE_{EL} is the value of the external quantum efficiency of electroluminescence measured under the dark state conditions. The EQE_{EL} of the active layer of an OSC device is closely related to the molecular structures of the active layer materials and film-morphologies. Especially, the EQE_{EL} is closely related to the structures of the acceptors and their luminescent properties, so the addition of a guest acceptor component can effectively tune the electroluminescence efficiency of the active layer. To reduce the non-radiative recombination loss of an OSC means to increase the EQE_{EL}, which is determined by the following equation (Eq. 3) [23]:

$$EQE_{EL} = f_{e-h} \times \beta \times \eta_{PLQY} \times f_{outcoupling} \quad (3)$$

where $f_{e\text{-}h}$ is the probability of balanced charge injection, β is the probability of forming a correlated electron-hole pair or exciton from each pair of injected carriers, η_{PLQY} is the photoluminescence quantum yield (PLQY), and $f_{outcoupling}$ is the optical outcoupling coefficient. The ternary or quaternary strategy, *i.e.*, the addition of one or two guest (donor/acceptor) components into the binary blended active layer, is used to optimize the molecular stacking of the co-blended film, reduce the energetic disorder of the device and enhance the luminescence properties of the active layer, which in turn can effectively reduce non-radiative recombination. In this regard, Li *et al.* assumed from the theoretical calculation that a high PLQY value of 2% combined with an active layer absorption edge at about 900 nm would allow the optimized device to achieve a 20% PCE (Fig. 1b) [24].

3. The key roles of guest acceptors in reducing voltage loss

Reducing the voltage loss is one way to improve the PCE. The optimized fullerene derivative based devices, which generally exhibited E_{loss} values of about 0.80 eV, showed PCEs below 11%. For the ITIC-like fused-ring acceptors, the E_{loss} values of their optimized devices were reduced to around 0.70 eV, the V_{OC}s were typically around 0.83 V and the PCEs were increased to 15%. With the appearance of the Y-series acceptors, the efficiencies of the optimized devices increased to 15%–19% and the E_{loss} values were reduced to below 0.60 eV with V_{OC} in the range of 0.83–0.87 V [25]. In this section, it is revealed that the guest acceptors play a key role in reducing the voltage loss and increasing the V_{OC} by focusing the miscibility of the guest acceptor structures with the main binary blended D or A materials, the luminescence properties and the energetic disorder of the active layer, respectively. Table 1 summarizes the device parameters of various binary and ternary/quaternary OSCs with guest acceptors incorporated. Table 2 collects the voltage and voltage losses of ternary/quaternary OSCs with guest acceptors incorporated.

Fig. 2 shows the scattering plots of V_{loss}, ΔE_2 and ΔE_3 *vs.* V_{OC} of the binary and ternary/quaternary devices with guest acceptors

Table 1
Collections on device parameters for various binary and ternary/quaternary OSCs with guest acceptors incorporated.

No.	Active layer	Guest	Binary					Ternary/quaternary					Ref.
			Ratio	V_{OC} (V)	J_{SC} (mA/cm^2)	FF (%)	PCE (%)	Ratio	V_{OC} (V)	J_{SC} (mA/cm^2)	FF (%)	PCE (%)	
1	PM6:Y6	IDIC-C4Ph	1:1.2	0.83	25.88	72.23	15.61	1:1.2:0.15	0.87	26.65	77.85	18.10	[32]
2	PM6:Y6	FINIC	1:1.2 (BHJ)	0.855	25.7	72.7	16.0	1:0.9:0.3 (BHJ)	0.886	26.2	72.8	16.9	[33]
			1:1.2 (SHJ)	0.858	25.8	73.5	16.3	1:0.9:0.3 (SHJ)	0.887	26.8	74.7	17.8	
3	PM6:Y6	AQx-3	1:1.2	0.856	25.73	76.8	16.94	1:0.8:0.4	0.870	26.82	77.2	18.01	[35]
4	D18-Cl:Y6	Y6-1O	1:1.6	0.881	25.53	75.88	17.07	1:1.12:0.48	0.900	25.87	76.92	17.91	[36]
5	PM6:BTP-4F	BTP-2F	1:1.2	0.829	26.40	74.20	16.64	1:0.9:0.3	0.846	26.16	76.25	17.28	[38]
6	PM6:Y6	BTP-M	1:1.2	0.844	24.67	74.96	15.61	1:0.96:0.24	0.875	26.56	73.46	17.03	[39]
7	PM6:BTP-eC9	MOIT-M	1:1.2	0.84	27.0	76.1	17.4	1:1.2:0.3	0.87	27.4	77.3	18.5	[40]
8	PM6:BTP-eC9	BTP-F	1:1.2	0.845	26.81	77.5	17.58	1:1.05:0.15	0.858	26.99	79.7	18.45	[41]
	PM6:Y6	Y6-F	1:1.2	0.839	25.86	76.3	16.55	–	0.852	26.49	77.3	17.45	
	D18-Cl:L8-BO	L8-BO-F	1:1.6	0.888	25.10	77.8	17.37	–	0.902	25.30	78.3	17.83	
9	PM6:BTP-eC9	L8-BO-F	1:1.2	0.840	26.62	78.1	17.46	1:1.02:0.18	0.853	27.35	80.0	18.66	[42]
10	PM6:Y6	TPIIC	1:1.2	0.840	26.2	72.0	15.8	1:1.05:0.15	0.861	27.5	74.4	17.7	[51]
11	PM6:Y6	SN	1:1.2	0.83	25.96	76.2	16.5	1:1:0.2	0.83	27.63	75.9	17.5	[52]
12	PM6:BTP-eC9	HDO-4Cl	1:1.2	0.846	26.58	78.50	17.65	1:1:0.2	0.866	27.05	80.51	18.86	[53]
13	PBDB-T:Y14	SM16	1:1	0.830	27.31	70.22	15.91	1:1:0.1	0.844	27.49	73.60	17.09	[54]
14	PM6:BTP-BO-4F	BTA1	1:1.2	0.848	25.72	76.51	16.73	1:1.08:0.12	0.872	25.69	76.42	17.12	[55]
		BTA2							0.869	26.76	78.55	18.27	
		BTA3							0.863	26.46	77.87	17.78	
15	PBQx-TCl:BTP-eC9	BTA3	1:1.2	0.82	26.0	75.2	16.0	1:1:0.2	0.84	26.9	79.6	18.0	[56]
16	PBQx-TF:eC9-2Cl	F-BTA3	1:1.2	0.868	25.9	78.6	17.7	1:1:0.2	0.879	26.7	80.9	19.0	[57]
17	PM6:L8-BO	BTP-H2	1:1.2	0.877	26.32	80.3	18.5	1:0.9:0.3	0.892	26.68	80.7	19.2	[58]
18	PM6:Y6	BTP-S2	1:1.2	0.842	26.05	72.03	15.79	1:0.96:0.24	0.880	26.20	75.80	17.43	[59]
19	PM6:BO-4Cl	BO-5Cl	1:1.2	0.841	26.03	79.4	17.43	1:0.96:0.24	0.874	26.93	78.8	18.56	[60]
20	PM1:L8-BO	BTP-2F2Cl	1:1.2	0.893	26.20	79.13	18.51	1:1:0.2	0.881	27.15	80.14	19.17	[61]
21	PM6:BTP-eC9	BTP-S9	1:1.2	0.845	27.57	77.95	18.0	1:0.6:0.6	0.861	27.50	79.34	18.8	[66]
22	PM6:L8-BO	BTP-S10	1:1.2	0.880	26.16	79.34	18.30	1:0.96:0.24	0.898	26.80	80.22	19.26	[67]
23	PM6:BTP-eC9	L8-BO/BTP-S10	1:1.2	0.845	27.59	78.49	18.32	1:0.6:0.6	0.864	27.04	78.87	18.37	[68]
								1:0.5:0.5:0.2	0.883	27.17	80.49	19.32	

Table 2
Collections on voltage and voltage losses of ternary/quaternary OSCs with guest acceptors incorporated.

No.	Active layer	Guest	Binary						Ternary/quaternary						Ref.
			V_{OC} (V)	ΔE_1 (eV)	ΔE_2 (eV)	ΔE_3 (eV)	EQE_{EL} (10^{-4})	E_{loss} (eV)	V_{OC} (V)	ΔE_1 (eV)	ΔE_2 (eV)	ΔE_3 (eV)	EQE_{EL} (10^{-4})	E_{loss} (eV)	
1	PM6:Y6	IDIC-C4Ph	0.83	0.26	0.04	0.25	0.53	0.55	0.87	0.26	0.04	0.23	1.2	0.53	[32]
2	PM6:Y6	FINIC(BHJ)	0.855	0.252	0.009	0.206	7.5	0.496	0.886	0.255	0.006	0.238	2.7	0.470	[33]
		(SHJ)	0.858	0.252	0.017	0.224	1.3	0.493	0.887	0.255	0.002	0.212	2.1	0.469	
3	PM6:Y6	AQx-3	0.856	–	–	–	–	0.484	0.870	–	–	–	–	0.470	[35]
4	D18-Cl:Y6	Y6-1O	0.881	0.383	0.034	0.180	–	0.597	0.900	0.367	0.040	0.175	9.96	0.582	[36]
5	PM6:BTP-4F	BTP-2F	0.829	–	–	0.24	0.754	–	0.846	–	–	0.21	–	–	[38]
6	PM6:Y6	BTP-M	0.844	–	–	–	–	0.49	0.875	–	–	–	–	0.45	[39]
7	PM6:BTP-eC9	MOIT-M	0.84	0.26	0.04	0.24	0.82	0.54	0.87	0.26	0.05	0.21	2.99	0.52	[40]
8	PM6:BTP-eC9	BTP-F	0.845	0.269	0.071	0.209	2.35	0.549	0.858	0.272	0.070	0.198	3.66	0.540	[41]
9	PM6:BTP-eC9	L8-BO-F	0.840	0.263	0.054	0.211	2.2	0.528	0.853	0.267	0.053	0.199	3.5	0.519	[42]
10	PM6:Y6	TPIIC	0.840	0.253	0.055	0.239	0.95	0.547	0.861	0.253	0.066	0.216	2.10	0.535	[51]
11	PM6:Y6	SN	0.83	0.27	0.08	0.24	–	0.59	0.83	0.27	0.08	0.22	–	0.57	[52]
12	PM6:BTP-eC9	HDO-4Cl	0.846	0.26	0.08	0.21	2.80	0.55	0.866	0.26	0.08	0.19	5.30	0.53	[53]
13	PBDB-T:Y14	SM16	0.830	–	–	0.263	–	–	0.844	–	–	0.226	–	–	[54]
14	PM6:BTP-BO-4F	BTA1	0.848	0.262	0.050	0.241	–	0.553	0.872	0.262	0.047	0.220	2.0	0.529	[55]
		BTA2							0.869	0.262	0.045	0.225	1.7	0.532	
		BTA3							0.863	0.262	0.048	0.227	1.5	0.537	
15	PBQx-TCl:BTP-eC9	BTA3	0.82	–	–	0.23	1.4	–	0.84	–	–	0.22	2.4	–	[56]
16	PBQx-TF:eC9-2Cl	F-BTA3	0.868	0.264	0.069	0.229	1.45	0.562	0.879	0.264	0.066	0.219	2.09	0.551	[57]
17	PM6:L8-BO	BTP-H2	0.877	0.283	0.067	0.213	3.08	0.563	0.892	0.284	0.078	0.196	5.48	0.558	[58]
18	PM6:Y6	BTP-S2	0.842	0.26	0.07	0.25	0.44	0.58	0.880	–	–	–	–	0.54	[59]
19	PM6:BO-4Cl	BO-5Cl	0.841	0.276	0.042	0.221	1.4	0.539	0.874	0.276	0.028	0.192	4.6	0.496	[60]
20	PM1:L8-BO	BTP-2F2Cl	0.893	0.254	0.099	0.202	3.42	0.556	0.881	0.253	0.097	0.197	4.05	0.547	[61]
21	PM6:BTP-eC9	BTP-S9	0.845	0.251	0.071	0.217	1.78	0.539	0.861	0.250	0.048	0.203	2.95	0.501	[66]
22	PM6:L8-BO	BTP-S10	0.880	0.257	0.092	0.207	–	0.556	0.898	0.257	0.086	0.199	–	0.542	[67]
23	PM6:BTP-eC9	L8-BO/BTP-S10	0.845	0.252	0.065	0.210	2.61	0.528	0.864	0.255	0.109	0.194	5.23	0.558	[68]
									0.883	0.255	0.097	0.191	5.77	0.543	

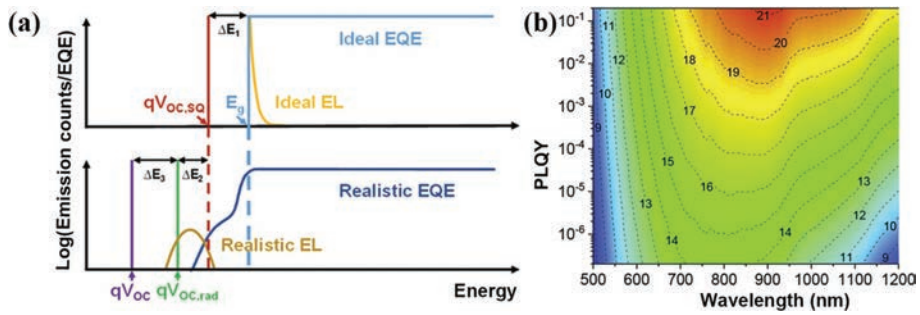

Fig. 1. (a) Schematic diagram of energy loss. Copied with permission [22]. Copyright 2020, Wiley Publishing Group. (b) Efficiency prediction for nonfullerene acceptors based OSCs with small energy offsets. Copied with permission [24]. Copyright 2020, Elsevier Publication Group.

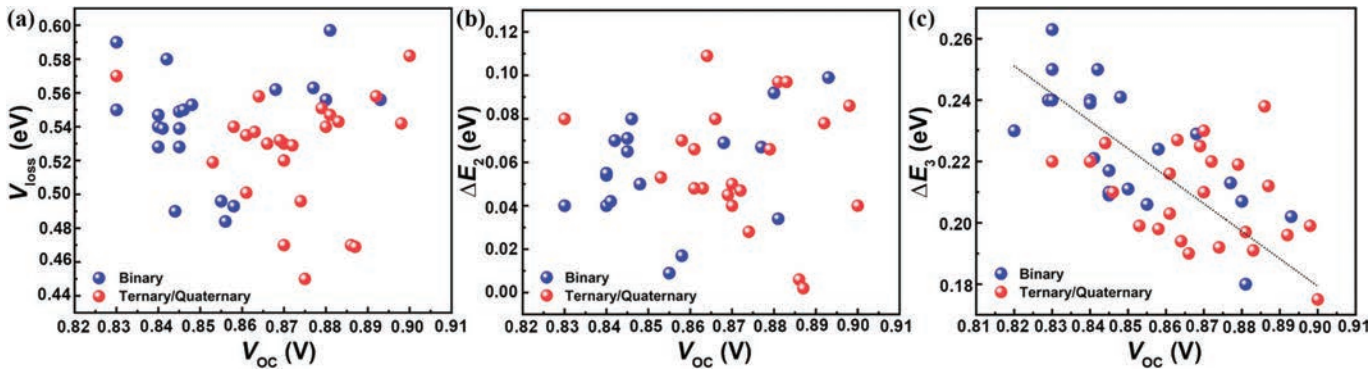

Fig. 2. The diagrams show the scattering plots of (a) V_{loss}, (b) ΔE_2, and (c) ΔE_3 *vs.* V_{OC} for the ternary/quaternary OSCs with guest acceptors incorporated.

(Fig. 3) incorporated. Compared to the binary devices, the scattering points for the ternary/quaternary devices after incorporating the guest acceptor material all show a rightward shift and a downward trend, indicating that the ternary/quaternary strategy can effectively reduce the voltage loss and achieve an open-circuit voltage increase. Interestingly, the ΔE_3 values show a trend decreased with the increase of V_{OC} and most of the ternary and quaternary devices show ΔE_3 values below 0.23 eV (Fig. 2c).

3.1. Miscibility

Miscibility is essentially defined as enthalpic variation with mixing two components and is therefore related to its intrinsic structural differences. For organic materials, the surface energies (γ) of two materials can be characterized by contact angle measurements, where two materials with similar surface energies are usually well miscible with each other [26]. In addition, the Flory-Huggins interaction parameter (χ) can be calculated based on the formula $\gamma_{A-B} \propto K(\sqrt{\gamma_A} - \sqrt{\gamma_B})^2$, where a larger value of χ indicates poor miscibility between the two materials and a smaller value of χ indicates good miscibility [27]. Furthermore, differential scanning calorimetry (DSC) is widely used to study physical changes in substances, such as glass transition temperature (T_g), melting temperature (T_m), crystallization temperature (T_c), crystalline transformations. In the polymer, the degree of miscibility between the materials is judged by observing whether the blends have a single T_g on the DSC curve. A single T_g on the DSC curve indicates that the two polymers are well miscible; if the blend has two T_g values, but both are between the T_g values of the two pure polymers, it means that the two polymers are somewhat miscible; if the two T_g values are the same as the T_g of the two pure polymers, respectively, it means that they are completely non-miscible and in a state of phase separation. Moreover, the change in miscibility and crystallinity between materials can be determined by the change in melting point, crystallinity point and enthalpy of the material and the blended material [28]. Solution processed binary OSCs in which excessive miscibility between the donor and acceptors results in poor phase separation, leading to severe carrier recombination; while poor miscibility in turn leads to larger phase separation, which is not favorable for exciton dissociation [29]. On the one hand, the molecular structures can be designed to adjust the dissolution of the molecules; on the other hand, a ternary or quaternary OSC can be constructed, with the addition of guest material to maintain the good morphology of the original binary blend and further fine-tune the phase size, phase purity, crystallinity and molecular stacking of the binary blend. Both strategies are effective to tune miscibility and to achieve optimization of the morphology and regulation of the phase separation.

The accurate location of the guest material in the blend film can be predicted by calculation of the wetting coefficient (ω) from the interfacial surface energy based on Young's equation and Neumann's equation [30,31]. If $\omega < -1$, it is located in the acceptor phase. If $-1 < \omega < 1$, it will be at the donor/acceptor interface. If $\omega > 1$, it is located in the donor phase. When the added guest components are distributed into the host donor (acceptor) phase, an alloy-like phase can usually be formed. The alloy-like phase formation facilitates the achievement of a more ordered molecular orientation, a more moderate degree of crystallinity and a more optimized morphology, which is beneficial for enhanced charge separation and transport as well as reduced charge recombination, reduced voltage losses and increased open-circuit voltage.

Zhu *et al.* used A-D-A type wide-bandgap IDIC-C4Ph (Fig. 3) with high LUMO energy level as the guest acceptor to build the PM6:Y6:IDIC-C4Ph ternary system and compared the χ values, where the χ value for Y6:IDIC-C4Ph was 0.25 K, being smaller than that of PM6:Y6 (0.44 K) and that of PM6:IDIC-C4Ph (1.34 K). This indicates that IDIC-C4Ph had better miscibility with Y6 and facilitated the formation of the acceptor alloy phase in the ternary system. The EQE_{EL} of the device was increased from 5.3×10^{-5} for binary devices to 1.2×10^{-4} for ternary devices, and the V_{OC} of

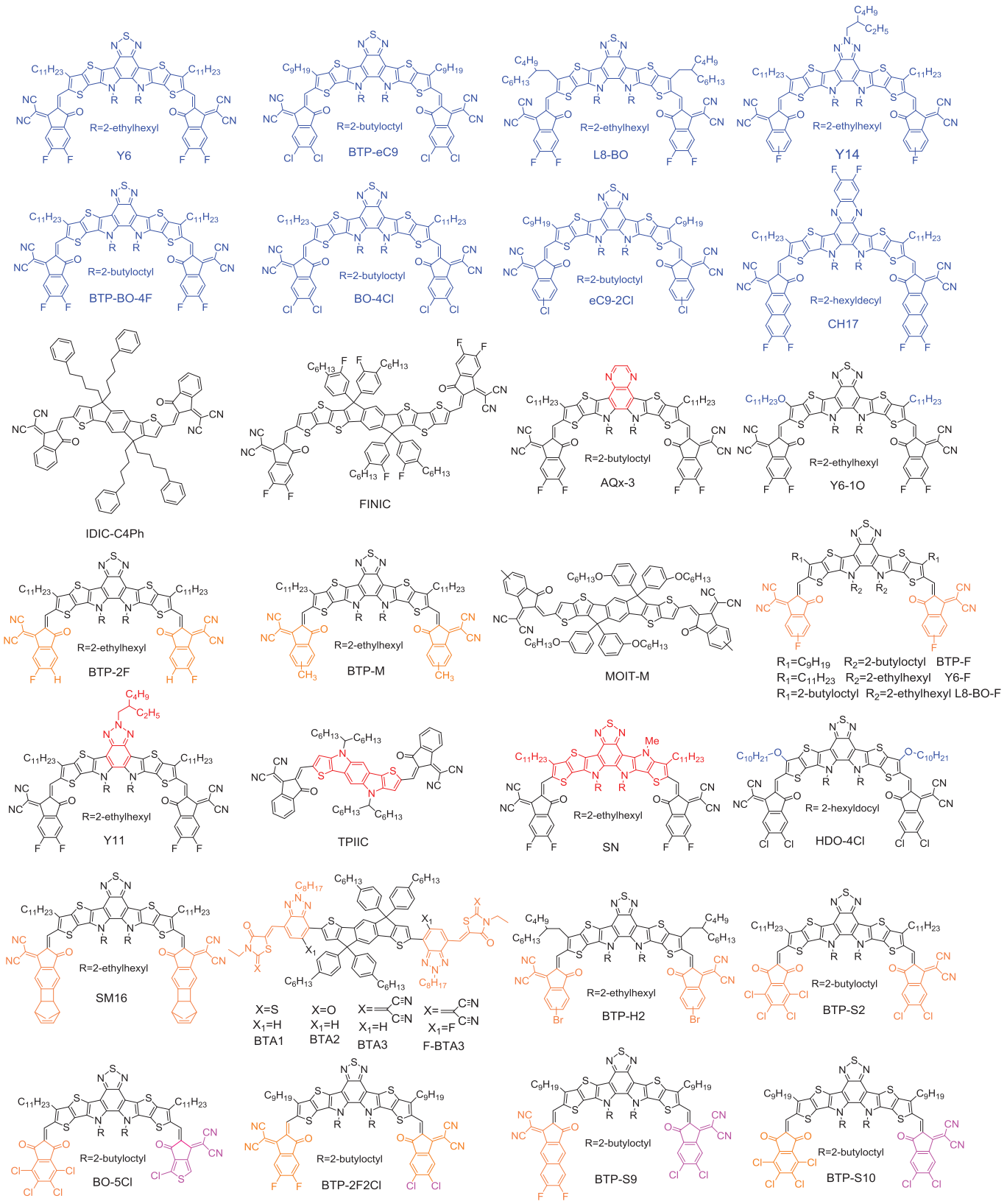

Fig. 3. Chemical structures of acceptors mentioned in this review.

the device from 0.83 V to 0.87 V. The formation of the alloy-like phase also improved the carrier transport and collection properties and reduced the recombination losses. The J_{SC} and FF were simultaneously improved, and the ternary device obtained a PCE of 18.10% [32]. Zhan *et al*. used FINIC (Fig. 3) as a guest acceptor for PM6:Y6. FINIC had a similar γ values to Y6 (36.3 mN/m *vs*. 33.7 mN/m), $\chi_{Y6:FINIC}$ is 0.0483, which demonstrated good miscibility between them. The addition of the guest acceptor reduced non-radiative recombination losses (0.206 eV *vs*. 0.238 eV), achieved an increase in V_{OC} from 0.855 V to 0.886 V and J_{SC} from 25.7 mA/cm^2 to 26.2 mA/cm^2, and gave a PCE of 16.9% for the ternary device. A sequential processed heterojunction structure (SHJ) was also used to investigate the vertical phase distribution of the co-hybrid film, gave an efficiency of 17.8% for the ternary device [33].

Many studies have shown that two non-fullerene acceptors with highly similar molecular structures facilitate good miscibility/compatibility between the materials, and by adjusting the miscibility between the host and the guest, an alloy-like phase can be formed or the phase purity of the main binary can be adjusted [34]. Thus, a series of Y6 derivatives with the same structures as Y6 have been developed and used for the guest components. For example, Zhu *et al*. synthesized the AQx-3 (Fig. 3) acceptor and introduced it into the PM6:Y6 system, where the high structural similarity and good miscibility of AQx-3 with Y6 resulted in the formation of an alloy-like phase. A small energy shift between the donor and acceptor alloys was formed, which achieved a reduction in energy loss, enhanced the hole transfer, suppressed charge recombination and optimized the morphology. The J_{SC} (25.73 mA/cm^2 *vs*. 26.82 mA/cm^2) and FF (76.8% *vs*. 77.2%) were improved while ensuring a V_{OC} (0.856 V *vs*. 0.870 V) enhancement, yielding a PCE of 18.01% [35]. Zhang *et al*. used Y6–1O (Fig. 3) with an asymmetric outer side chain as a guest acceptor for the D18-Cl:Y6 binary system. The similar structures between Y6 and Y6–1O resulted in good miscibility and the formation of a Y6:Y6–1O alloy-like phase. The ternary strategy improved the EQE_{EL} of the device and minimized energy loss (0.597 eV *vs*. 0.582 eV). The V_{OC} was increased from 0.881 V for the binary devices to 0.900 V for the ternary device, obtaining an efficiency of 17.91% [36].

The phase purity of the mixed phase is also very important for the device's performance. An impure phase region will have excessive charge recombination. Phase with too much purity is good for charge transport but not for exciton dissociation due to the lack of sufficient D/A interface and phase with high purity is not favorable for obtaining high efficiency [37]. Hereby, Ma *et al*., used BTP-2F (Fig. 3) and BTP-4F as two similar non-fullerene acceptors in a ternary blend to construct a pseudo-binary system to modulate acceptor composition and donor-acceptor (D-A) miscibility. The addition of the guest acceptor was found to increase domain purity (Figs. 4a and b), increase EQE_{EL} and reduce non-radiative recombination loss (0.24 eV *vs*. 0.21 eV). The ternary device gave an efficiency of 17.28% [38]. Chen *et al*. synthesized BTP-M (Fig. 3) by replacing IC-2F of Y6 with a monomethyl-substituted IC and introduced it into the PM6:Y6 binary system. Contact angle, DSC, and cyclic voltammogram (CV) measurements showed that BTP-M and Y6 were well miscible and an alloy-like acceptor phase was formed between them. A balance between V_{OC} and J_{SC} was achieved. Also, the introduction of BTP-M effectively suppressed the strong aggregation behavior of Y6 with reduced energy loss (0.49 eV *vs*. 0.45 eV), achieved a PCE of 17.03% for the ternary device [39].

The above strategies are also suitable for the binary system of Y6 derivatives. For example, Zhang *et al*. incorporated MOIT-M (Fig. 3) into the PM6:BTP-eC9 binary system. Photoluminescence studies showed the presence of energy transfer from MOIT-M to BTP-eC9. $\chi_{PM6:BTP\text{-}eC9}$, $\chi_{PM6:MOIT-M}$ and $\chi_{BTP\text{-}eC9:MOITI-M}$ were of 0.10 K, 0.31 K and 0.06 K, respectively, while the calculated wetting coefficient (ω) of MOIT-M in PM6:BTP-eC9 was −2.59, indicating that MOIT-M was located in the acceptor phase and MOIT-M formed a well-mixed phase with BTP-eC9, and the addition of the guest acceptor reduced the non-radiative recombination loss (from 0.24 eV to 0.21 eV), obtained a V_{OC} of 0.87 V, with a final 18.5% PCE obtained for the ternary device [40]. Sun *et al*. synthesized BTP-F (Fig. 3) by mono-fluorinating the host acceptor end group and incorporated it as a guest acceptor into the PM6:BTP-eC9 binary blend. Such a change in the molecular structure achieved fine-tuning of the energy levels while ensuring miscibility. The addition of the guest improved the ordering of the molecular stacking, optimized the active layer morphology, reduced the non-radiative recombination (0.209 eV *vs*. 0.198 eV), increased the V_{OC} from 0.845 V to 0.858 V, increased the FF from 77.5% to 79.7%, and gave an efficiency of 18.45%. With this strategy, the Y6-F and L8-BO-F (Fig. 3) acceptors were synthesized and used as guest components of PM6:Y6, D18-Cl:L8-BO binary blends, respectively, and the PCEs of the devices were both enhanced [41]. The addition of L8-BO-F to the PM6:BTP-eC9 co-blend enhanced the EQE_{EL} value (3.5×10^{-4} *vs*. 2.2×10^{-4}), reduced the non-radiative recombination loss (0.211 eV *vs*. 0.199 eV), and achieved a simultaneous enhancement in V_{OC} (0.840 V *vs*. 0.853 V), J_{SC} (26.62 mA/cm^2 *vs*. 27.35 mA/cm^2), and FF (78.1% *vs*. 80.0%) with the ternary device achieving a PCE of 18.66% [42].

These studies show that through the molecular design strategy of guest acceptors in combination with the ternary-quaternary strategy, the adjustment of the miscibility between the materials and the adjustment of the phase purity, crystallinity, molecular stacking mode and phase separation can be effectively achieved to reduce the energy loss and further improve the open-circuit voltage and obtain the efficiency improvement.

3.2. Luminescence performance tuning

According to Eq. 3, the improved luminescent performance of an OSC device is beneficial to maximizing the V_{OC}, while the luminescent characteristics of the device are mainly determined by the narrow bandgap material, thus increasing the PLQY of the narrow bandgap acceptor can suppress the non-radiative voltage loss in the organic solar cell due to the hybridization between the singlet state and the CT state [43,44]. Due to the easy modification of the structures of the non-fullerene acceptors, the luminescent properties of the materials can be enhanced by introducing luminescent groups such as pyrrole, halogen and asymmetric structures into the molecules, which regulates the molecular stacking behavior and alleviates fluorescence quenching [45,46]. Again, the luminescent properties of the materials can be also enhanced by replacing benzothiadiazole (BT) with benzotriazole (BTA). For example, Zou *et al*. by replacing the Y6 central core BT with a BTA, synthesized Y11 (Fig. 3). The weak electron-withdrawing characteristic of the BTA unit reduced the bandgap and achieved a much higher PLQY value of 1.3×10^{-3} for the binary active layer co-blended with the polymer donor PM6, achieving a nearly ∼5 times increase in PLQY compared to the PLQY of Y6 (2.8×10^{-4}). Based on PM6:Y11, the binary device obtained an ΔE_3 as low as 0.20 eV [47,48].

There is a balance between charge transport and light emission in the luminescent layer, and highly luminescent materials may disrupt the ordering of the molecular stack to the disadvantage of charge transport, resulted in unbalanced V_{OC}, J_{SC} and FF, making it difficult to maximize efficiency [49,50]. Therefore, the ternary and quaternary OSCs are effective approaches to tune the luminescence of the active layers, by adding or replacing part of the main acceptors with a small amount of high luminescence guests in the active layers of a high-performance binary OSCs, to balance the relationship between charge transport and light emission, to achieve a reduction in non-radiative recombination loss and to achieve a synergistic improvement of V_{OC}, J_{SC} and FF.

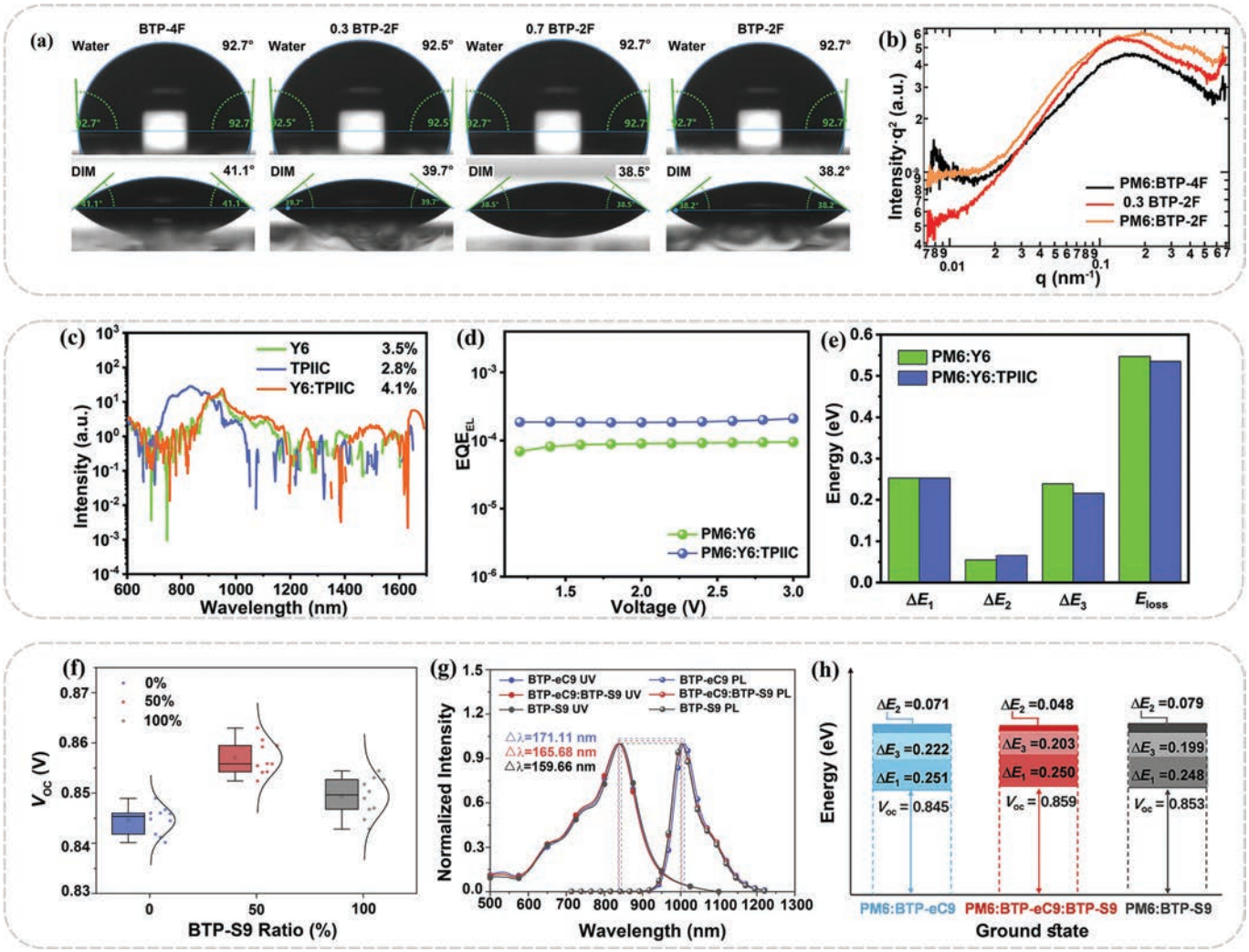

Fig. 4. (a) Contact angles of the BTP-XF mixtures. (b) R-SoXS profiles at 284.8 eV of BTP-XF the blends. Copied with permission [38]. Copyright 2022, Wiley Publishing Group. (c) FTIR spectra of Y6, TPIIC, and Y6:TPIIC films. (d) Electroluminescence quantum efficiency profiles of PM6:Y6 and PM6:Y6:TPIIC based binary and ternary OSCs at different applied voltages. (e) E_{loss} and its exhaustive three parts of ΔE_1,ΔE_2 and ΔE_3 values of PM6:Y6 and PM6:Y6:TPIIC based binary and ternary OSCs. Copied with permission [51]. Copyright 2022, Royal Society of Chemistry. (f) Statistical data of V_{OC} for OPVs with various BTP-S9 ratios. (g) Reorganization energy variations among binary and ternary systems. (h) Statistical data of Voltage loss for OPVs with various BTP-S9 ratios. Copied with permission [66]. Copyright 2022, Elsevier Publication Group.

Min *et al.* used the TPIIC (Fig. 3) with a high LUMO energy level as a guest acceptor for the PM6:Y6 system, formed a cascade energy level design. A PLQY of 4.2% was obtained based on Y6:TPIIC when replaced the Y6 with the TPIIC component at a weight ratio of 0.15, which was higher than the PLQY values of Y6 (3.5%) and TPIIC (2.8%) pure films (Fig. 4c). The improved luminescent performance resulted in an increase in EQE_{EL} values from 9.5×10^{-5} for the PM6:Y6 binary devices to 2.1×10^{-4} for the ternary device (Fig. 4d). Thus, the calculated ΔE_3 values were 0.216 eV and 0.239 eV for the ternary and binary devices, respectively, which meant that the addition of TPIIC reduced the non-radiative energy loss (Fig. 4e). Meanwhile, the 1.05:0.15 co-blended Y6:TPIIC film exhibited a relatively larger crystal coherence length (CCL) (20.8 Å *vs.* 21.29 Å) and a longer carrier lifetime. While gaining an improved V_{OC} (0.840 V *vs.* 0.861 V), the simultaneous improvement in J_{SC} (26.2 mA/cm^2 *vs.* 27.5 mA/cm^2) and FF (72.0% *vs.* 74.4%) was obtained, yielding an efficiency of 17.7% [51].

Zhu *et al.* introduced an N atom into the Y6 conjugated backbone to synthesize an asymmetric non-fullerene acceptor, SN (Fig. 3). SN (1.95%) exhibited a higher PLQY than Y6 (1.77%). To introduce it into the PM6:Y6 binary system effectively reduced the non-radiative voltage loss (0.24 eV *vs.* 0.22 eV) and the ternary devices of PM6:Y6:SN obtained a PCE of 17.5% [52].

Hou *et al.* used HDO-4Cl (Fig. 3) as a guest acceptor for PM6:BTP-eC9. When the 0.2 wt ratio of BTP-eC9 was replaced with the HDO-4Cl component, the PLQY of the BTP-eC9:HDO-4Cl was higher (4.2%) than the PLQY value of the BTP-eC9 (2.3%) pure film. The addition of the guest acceptor increased the exciton diffusion length (12.2 nm *vs.* 16.3 nm), reduced the trap density of defect states, improved EQE_{EL} values (5.30×10^{-4} *vs.* 2.80×10^{-4}), and reduced non-radiative energy loss, while the co-blended film exhibited a relatively tighter π-π stacking (3.81 Å *vs.* 3.71 Å). While the V_{OC} achieved a 0.02 V improvement, the J_{SC} and FF also raised at the same time, with the ternary device obtaining an efficiency of 18.86% [53].

End-group engineering is a common means of molecular modification in photovoltaic materials and usually involves the introduction of halogen atoms or other aromatic structures to achieve a modulation of the molecular stacking pattern and photovoltaic properties.

Bo *et al.* designed and synthesized two acceptors SM16 (Fig. 3) and SM16-R, which bore an A–DA'D–A type backbone and two nor-

bornenyl modified 1,1-dicyanomethylene-3-indanone (IC) terminal groups. Compared to the SM16-R, the SM16 had a higher PLQY (8.61% *vs*. 6.27%). The PBDB-T:SM16-based binary device achieved a low non-radiative recombination loss of 0.145 eV and a high open-circuit voltage of 0.977 V. By adding it as a guest component to the PBDB-T:Y14 binary system, the non-radiative recombination loss was reduced (0.263 eV *vs*. 0.226 eV) and the ternary device achieved a simultaneous improvement in V_{OC} (0.830 V *vs*. 0.844 V), FF (70.22% *vs*. 73.60%), and PCE (15.91% *vs*. 17.09%) [54].

Chen *et al*. synthesized BTA1–3 (Fig. 3) with IDT as the D unit, benzotriazole as the A1 unit and with different electron-withdrawing capabilities (rhodanine R, thiazolidine-2,4–dione TD and 2-(1,1-dicyanomethylene) as the end groups, respectively. That 10 wt% weight ratio of BTA1–3 was added to PM6:BTP-BO-4F binary system showed higher EQE_{EL} values of 2.0×10^{-4}, 1.7×10^{-4} and 1.5×10^{-4}, achieving ΔE_3 values of 0.220, 0.225 and 0.227 eV, respectively. Also, the devices after incorporating BTA1–3 exhibited more efficient exciton dissociation, improved charge transport and reduced charge recombination, which improved J_{SC} and FF, yielding PCEs of 17.12%, 18.27% and 17.78%, respectively [55].

Hou *et al*. synthesized a polymer donor with highly luminescent properties, PBQx-TCl, which was co-blended with BTP-eC9 to give a PCE of 16.0%. Added BTA3 as a guest acceptor to the PBQx-TCl:BTP-eC9 binary system enhanced the EQE_{EL}, increased the V_{OC} from 0.82 V to 0.84 V and the FF significantly from 75.2% to 79.6%. The final ternary device obtained 18.0% PCE [56]. Then, PBQx-TF, eC9–2Cl and F-BTA3 (Fig. 3) were synthesized to optimize the solar spectral coverage and energy level alignment. By incorporating F-BTA3 as a guest acceptor into the PBQx-TF:eC9–2Cl binary system, the intermolecular stacking was enhanced, the EQE_{EL} was improved and the non-radiative recombination loss was reduced. Hence, the V_{OC} was enhanced from 0.868 V to 0.879 V, the J_{SC} from 25.9 mA/cm^2 to 26.7 mA/cm^2, and FF from 78.6% to 80.9%. The ternary device based on PBQx-TF:eC9–2Cl:F-BTA3 co-blend achieved a PCE of 19.0% [57].

Chen *et al*. synthesized BTP-H2 (Fig. 3) by brominating the end-groups of L8-BO, which was added as a guest acceptor to the PM6:L8-BO binary system. The addition of the guest acceptor enhanced the luminescence, increased the EQE_{EL} from 3.08×10^{-4} to 5.48×10^{-4} and reduced the non-radiative recombination loss from 0.213 eV to 0.196 eV. This is consistent with the improvement in V_{OC}, with the optimized device achieving a PCE of 19.2% [58].

Some research has shown that asymmetric fused-ring electron acceptors have larger dipole moments and stronger binding energies, led to increased intermolecular interactions. By adopting an asymmetric strategy, the photoelectric properties of acceptors and the molecular stacking can be subtly modified to modulate the aggregation behavior of the active layer.

Chen *et al*. by introducing six halogen atoms into the end groups of Y5 and removing the cyano-group at the end IC group bearing four chlorine atoms, synthesized BTP-S2 (Fig. 3), which had a blue-shifted absorption compared to Y6 with a bandgap of 1.41 eV and a LUMO energy level of −4.01 eV. The device based on the asymmetric BTP-S2 gave an EQE_{EL} of 2.3×10^{-4}, up to an order of magnitude higher than that of the device based on symmetric Y6 (4.4×10^{-5}), thus significantly reducing the non-radiative loss and energy loss of the device. The ternary device based on PM6:BTP-S2:Y6 (1:0.96:0.24) achieved an efficiency of 17.43% [59]. Then, by asymmetric design of the end groups, BO-5Cl (Fig. 3) was synthesized. Single crystal structure showed that BO-5Cl with a large dipole moment had a reduced π-π stacking distance between adjacent molecules compared to BO-4Cl (3.4 Å *vs*. 3.3 Å), resulting in a tighter stacking, while symmetric BO-4Cl showed a less stacking pattern. Such molecular arrangement pattern allowed BO-5Cl to obtain longer exciton lifetimes, stronger hybridization between CT and local exciton (LE) states and the presence of a double interfacial electronic manifold, resulting in BO-5Cl with high luminescence properties. Blending BO-5Cl with PM6 donor obtained a high EQE_{EL} of 0.1%. The addition of BO-5Cl as a guest acceptor to the PM6:BO-4Cl binary system enhanced the luminescence properties. An improved EQE_{EL} (1.4×10^{-4} *vs*. 4.6×10^{-4}) and a reduced non-radiative recombination loss (0.221 eV *vs*. 0.192 eV) were obtained. The ternary device gave a PCE of 18.56% [60].

Min *et al*. synthesized narrow bandgap BTP-2F2Cl (Fig. 3) by following the strategy of asymmetric chlorination on the end-groups and added it as a guest acceptor to the PM1:L8-BO binary blend system. The ternary device exhibited faster exciton dissociation at the D/A interface and exciton diffusion to the interface before dissociation and longer carrier lifetime than the binary devices. Compared to the L8-BO pure film, the L8-BO:BTP-2F2Cl co-blended film showed higher PLQYs (3.2% *vs*. 3.8%) and larger exciton diffusion lengths (4.98 nm *vs*. 6.33 nm). The ternary OSC showed reduced non-radiative recombination losses (0.202 eV *vs*. 0.197 eV) and gave an efficiency of 19.17% [61].

The above cases demonstrated that the introduction of high luminescent groups within the molecule or the asymmetric design on the end-groups can effectively regulate the luminescent properties of the material. Use of that material as a guest acceptor to build ternary or quaternary devices can achieve the tuning of the luminescent properties of the device, reduce the non-radiative recombination loss, and achieve the V_{OC} improvement.

3.3. Energetic disorder tuning

Organic semiconductor materials are generally amorphous and therefore they have a greater energetic disorder than inorganic semiconductors. The distribution of the density of states (DOS) may extend into the band gap region, leading to tail state absorption, which further brings about energetic disorder [48]. The presence of energetic disorder in this could increase the loss of radiative recombination below the band gap as well as lead to severe non-radiative recombination, both of which damage the V_{OC}. Blakesley and Neher proposed that energetic disorder (σ) in the transport energy level within the bulk-heterojunction (BHJ) played an important role in V_{OC} and that the voltage loss was directly related to $\sigma 2/k_BT$, where k_B is the Boltzmann constant and T is the temperature [62]. Therefore, reducing the σ value would achieve an increase in V_{OC}. It has been shown that molecular design strategies can be effective in reducing energy disorder [63,64]. For instance, Chen *et al*. synthesized CH17 (Fig. 5) by extending the conjugated system in both directions for the Y6 central and end-group units. The large conjugated extension fine-tuned the absorption and energy levels, provided a more optimized and stronger 3D molecular network and strong intermolecular stacking pattern. Again, it resulted in better charge transport, less radiative recombination, higher luminescent efficiency and reduced non-radiative recombination loss. Compared with Y6, the energetic disorder of the co-blended film was reduced considerably (23.1 meV *vs*. 20.8 meV) and gained an efficiency of 17.84% when blending with PM6 (Figs. 5a-f) [65].

Asymmetric design on guest acceptor molecule can also be used to achieve a reduced energetic disorder in the device, thereby improving device performance.

Chen *et al*. added asymmetric BTP-S9 (Fig. 3) to the PM6:BTP-eC9 binary blend. Urbach energy (E_U) values were of 22.89 meV, 23.39 meV and 21.79 meV for PM6:BTP-eC9, PM6:BTP-S9, and PM6:BTP-S9:BTP-eC9, respectively. The ternary device showed reduced recombination energy, reduced energetic disorder and improved luminescence efficiency, resulting in reduced ΔE_2 from 0.071 eV to 0.048 eV and ΔE_3 from 0.217 eV to 0.203 eV and increased V_{OC} for the ternary device (Figs. 4f-h). The ternary blend exhibited enhanced charge transport properties due to stronger π-π stacking and enhanced CCL than the binary film, resulting in

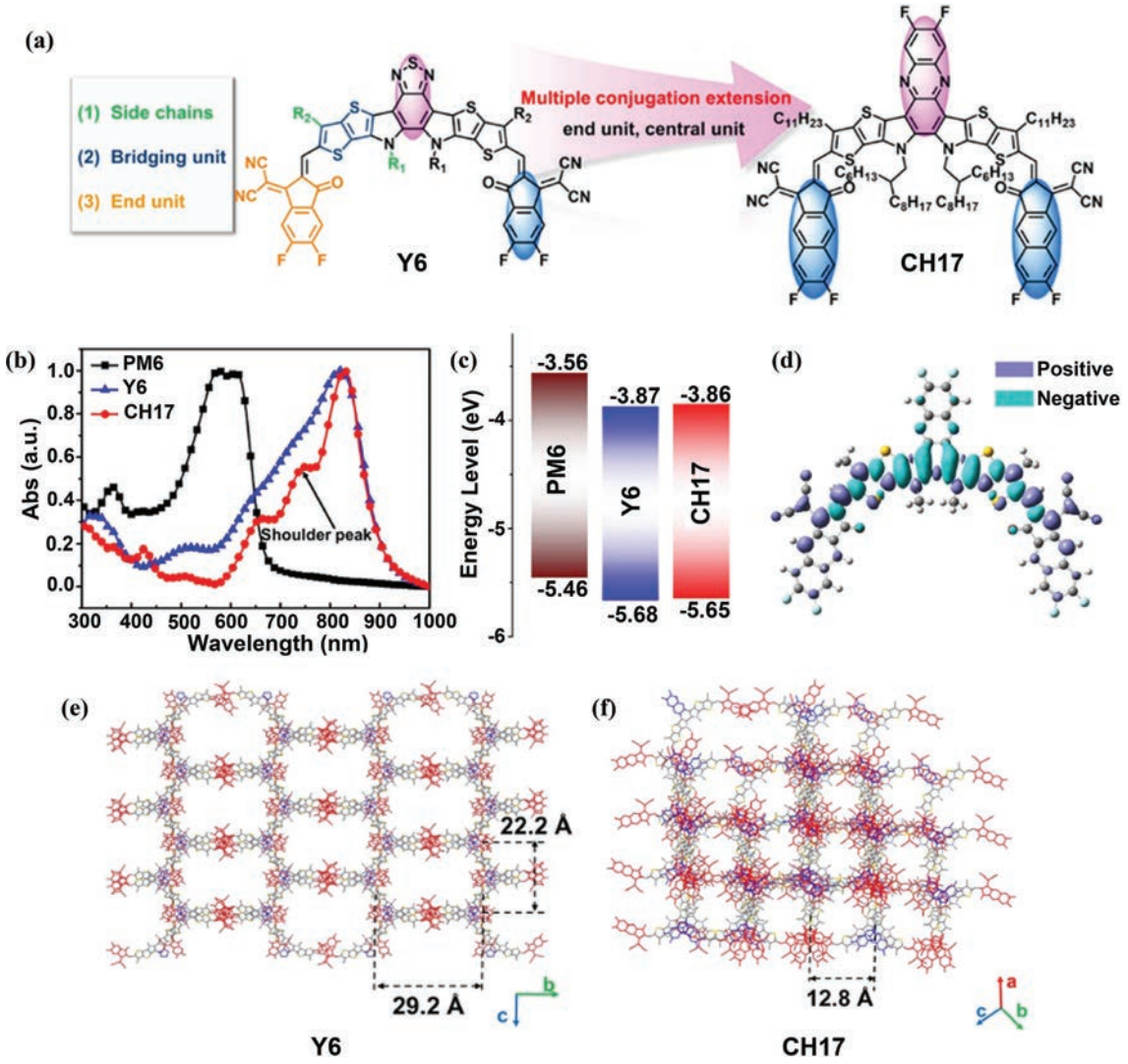

Fig. 5. (a) Molecular structures of Y6 and CH17. (b) Normalized absorption spectra of PM6, Y6 and CH17 films. (c) Energy levels diagram of PM6, Y6 and CH17 [65], and (d) isosurface of charge density difference (ΔQ) for CH17, where $\Delta Q = \Psi^2_{LUMO} - \Psi^2_{HOMO}$. (e, f) Single crystal structures of Y6 and CH17. Copied with permission. Copyright 2022, Springer Nature.

enhanced FF, with the ternary device gave a PCE of 18.8% [66]. They incorporated the asymmetric molecule containing six chlorine atoms at the end groups, *i.e.*, BTP-S10 (Fig. 3), as a guest acceptor into the PM6:L8-BO binary system. The ternary device exhibited a reduced E_U (25.71 meV *vs.* 25.40 meV) compared to the binary device and a reduced energy shift between CT state energy level (E_{CT}) and the local excited state energy level (E_{LE}) ($\Delta E_{LE\text{-}CT}$), which was consistent with the reduced ΔE_2 (0.092 eV *vs.* 0.086 eV) and ΔE_3 (0.207 eV *vs.* 0.199 eV). Improvement in device V_{OC} (0.880 V *vs.* 0.898 V) was achieved with simultaneously improved J_{SC} (26.16 mA/cm^2 *vs.* 26.80 mA/cm^2) and FF (79.34% *vs.* 80.22%). A PCE of 19.26% was achieved [67]. Thereafter, by constructing a quaternary device with PM6, BTP-eC9, L8-BO and BTP-S10, their electroluminescence spectroscopy and high-resolution Fourier transform photocurrent spectroscopy EQE spectra (FTPS-EQE) results showed that, compared to the ΔE_2 (0.109 eV) of the PM6:BTP-eC9:L8-BO ternary device, which produced a large E_{loss} (0.558 eV), the addition of BTP-S10 resulted in a reduction in energetic disorder (with an E_U of 25.99 eV), a reduction in Stokes shift to 117.3 nm, a reduction in ΔE_2, an increase in the EQE_{EL} and a simultaneous reduction in ΔE_3. The quaternary device exhibited a lower E_{loss} (0.543 eV), a higher V_{OC} (0.883 V), and an efficiency of 19.32% [68].

Based on the above results, it is shown that molecular design can effectively achieve the regulation of molecular luminescence and energetic disorder. This in combination with the ternary-quaternary strategy that has higher V_{OC} than the binary devices effectively reduces the radiative and non-radiative recombination loss, opening a way for breaking the open-circuit voltage limitation and giving the basis of research for the further improvement of the efficiencies of OSCs.

4. The key roles of guest donors for reducing voltage loss

Compared to the acceptor, the donor usually has a wider bandgap. By designing or selecting a donor with a wide band gap and a low HOMO energy level as the guest component, the absorption of the main binary system in the short wavelength region can be effectively compensated, thus improving the J_{SC} and V_{OC}. Donors also generally include two main groups: one is small-molecule donors, which have a well-defined molecular structure and high crystallinity, and which are easy to synthesize, having good repro-

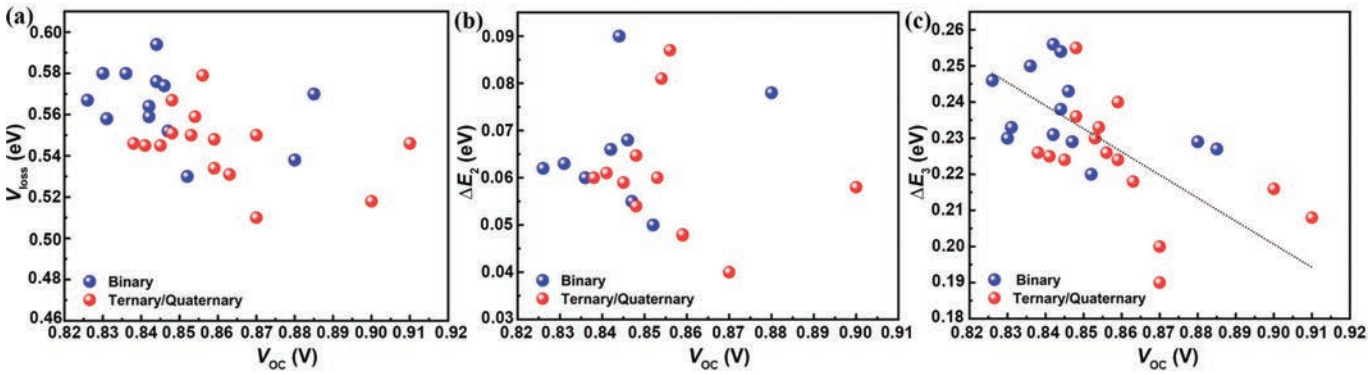

Fig. 6. The diagrams show the scattering plots of (a) V_{loss}, (b) ΔE_2, and (c) ΔE_3 *vs.* V_{OC} for the ternary/quaternary OSCs with guest donors incorporated.

ducibility and high purity. The other is polymer donors, which all show a strong tendency to aggregate and good dispersibility in solvents. The most advanced acceptor small-molecules are currently amorphous and when polymer donors are mixed, the aggregation of these donor polymers can limit the nucleation and growth of the acceptor, forming a phase with high purity and optimized morphology, while the high molecular weight of the polymer gives a major boost to the stability of the device. Table 3 shows the device parameters of various binary and ternary/quaternary OSCs with guest donors incorporated. Table 4 collects the voltage and voltage losses of ternary/quaternary organic solar cells with guest donor materials incorporated.

Fig. 6 shows the scattering plots of V_{loss}, ΔE_2 and ΔE_3 *vs.* V_{OC} for the binary and ternary/quaternary devices with guest donors (Fig. 7) incorporated. The ternary and quaternary devices after adding guest donors all exhibit increased open-circuit voltage, reduced voltage losses and non-radiated recombination losses compared to the base binary devices (The red points are all positioning at the bottom right.). Both V_{loss} and ΔE_3 show a trend decreasing with increasing V_{OC} (Fig. 6c).

4.1. Miscibility

Similar to the guest acceptor addition, the introduction of a polymer/small-molecule donor with a similar structure to the host donor into the host binary blend to obtain a well-miscible donor phase and the synergistic interaction between the guest donor and the host D:A combination by means of ratio adjustment leads to component-dependent changes in V_{OC} and J_{SC} and the formation of a good BHJ morphology to achieve performance parameter improvements. With the addition of a guest material, it is also possible to regulate the phase separation of the active layer. Benzo[1,2-*b*:4,5-*b*']dithiophene (BDT) is widely used in the design of donor bodies as an electron-rich unit and with a rigid planar conjugated structure that promotes π-π stacking and delocalized electron in the solid state, thereby facilitating charge transport [69].

Chen *et al*. introduced PTO2 (Fig. 7) as a guest donor in the binary systems based on PM6:Y6 and PM6:BTP-eC9 and constructed the corresponding ternary devices, respectively. $\chi_{PM6\text{-}PTO2}$, $\chi_{PM6\text{-}Y6}$, $\chi_{PM6\text{-}BTP\text{-}eC9}$, $\chi_{PTO2\text{-}Y6}$ and $\chi_{PTO2\text{-}BTP\text{-}eC9}$ of 0.01 K, 0.54 K, 0.11 K, 0.65 K and 0.16 K indicated that PM6-PTO2 had good miscibility and formed an alloy-like phase. The value of $\chi_{PTO2\text{-}Y6}$ is larger than that of $\chi_{PM6\text{-}Y6}$, indicating a higher degree of phase separation in the PTO2-Y6 mixture, which resulted in effective charge transfer and suppression of trap-assisted recombination. Also, the smaller energy shift between the donor mixture and Y6 resulted in lower ΔE_2 values (0.078 eV *vs.* 0.058 eV) and ΔE_3 values (0.229 eV *vs.* 0.216 eV) for the ternary devices, with 17.05% and 18.01% PCEs obtained for the Y6- and BTP-eC9-based ternary devices, respectively [70].

Liu *et al*. used PM7 (Fig. 7) and $PC_{71}BM$ as guests. PM7 had a similar chemical structure to PM6 and a deeper HOMO energy level (−5.24 eV *vs.* −5.13 eV) and $PC_{71}BM$ had a higher LUMO energy level than Y6 (−4.10 eV *vs.* −4.29 eV). They constructed a quaternary device with a dual cascade energy level design, which effectively improved electron transfer and separation with improved J_{SC}. The addition of the guest PM7 and $PC_{71}BM$ reduced the energy offset and suppressed the non-radiative recombination loss. The quaternary device of PM6:PM7:Y6:$PC_{71}BM$ (0.8:0.2:1.2:0.25) exhibited a minimum ΔE_2 value of 0.048 eV, yielding a reduction in energy loss from 0.564 eV in binary device to 0.548 eV in quaternary device and an improvement in V_{OC} by 0.017 V. The whole crystallization of the quaternary blend was improved compared to the binary and ternary blend films, resulting in increased electron and hole mobilities and improved FF. The quaternary device obtained 18.07% PCE (Figs. 8a-c) [21].

An *et al*. based on BDT units and synthesized a wide band gap polymer S3 (Fig. 7) with a lower HOMO energy level than PM6 (−5.50 eV *vs.* −5.48 eV), which was added as a guest donor to the PM6:Y6 binary system. S3 and PM6 showed good compatibility, formed an alloy-like phase with the ternary devices, and exhibited good film-morphology, which facilitated charge generation and extraction. Replacement of 0.2 wt ratio of PM6 by S3 yielded a reduced non-radiative recombination loss (0.238 eV *vs.* 0.226 eV) and the simultaneous enhancement in V_{OC} (0.844 V *vs.* 0.856 V), J_{SC} (25.13 mA/cm^2 *vs.* 25.86 mA/cm^2) and FF (75.85% *vs.* 79.17%) resulted in a 17.53% PCE [71].

Wang *et al*. synthesized PM6-Si30 (Fig. 7) by introducing chlorine and alkylsilyl groups onto the BDT units in PM6 and added it to the PM6:BTP-eC9 binary system. The terpolymer of PM6-Si30 formed an alloy phase with PM6. With replacement of 0.15 wt ratio of PM6 with PM6-Si30, the ternary blended film showed a decrease in the π-π stacking distance based on the OOP (010) peak and an increase in the CCL value (25.13 Å *vs.* 28.56 Å). At the same time, the addition of the guest donor reduced ΔE_2 (0.05 eV *vs.* 0.04 eV) and ΔE_3 (0.22 eV *vs.* 0.20 eV), achieved an increase in V_{OC} from 0.852 V to 0.870 V. The ternary device based on PM6:PM6-Si30:BTP-eC9 gave a PCE of 18.27% [72].

Hou *et al*. reported a wide band gap (2.12 eV) polymer donor based on thiadiazole, *e.g.,* PB2F (Fig. 7), with a deep HOMO energy level of −5.64 eV and a high EQE_{EL} of 3.9×10^{-3}. By incorporating it as a guest donor into PM6:BTP-eC9 binary blend and substituting PM6 with 0.2 PB2F, the EQE_{EL} of the ternary device increased to 2.2×10^{-4}, compared to the value of 1.3×10^{-4} in the PM6:BTP-eC9 binary device, meaning a reduction in the energy loss. The addition of the guest slightly improved the aggregation of the blended film while enhanced crystallinity, achieved more ef-

Table 3
Collections on device parameters for various binary and ternary/quaternary OSCs with guest donors incorporated.

No.	Active layer	Guest	Binary					Ternary/quaternary					Ref.
			Ratio	V_{OC} (V)	J_{SC} (mA/cm^2)	FF (%)	PCE (%)	Ratio	V_{OC} (V)	J_{SC} (mA/cm^2)	FF (%)	PCE (%)	
1	PM6:Y6	PTO2	1:1.2	0.88	24.95	67.18	15.05	1:0.1:1.2	0.90	25.53	72.80	17.05	[70]
	PM6:BTP-eC9		1:1.2	0.90	25.68	74.48	17.43	1:0.1:1.2	0.90	27.09	73.28	18.01	
2	PM6:Y6	PM7/PC_{71}BM	1:1.2	0.842	25.98	75.52	16.52	0.8:0.2:1.2	0.848	26.17	76.70	17.02	[21]
								0.8:0.2:1.2:0.25	0.859	26.55	79.23	18.07	
3	PM6:Y6	S3	1:1.2	0.844	25.13	75.85	16.08	0.8:0.2:1.2	0.856	25.86	79.17	17.53	[71]
4	PM6:BTP-eC9	PM6-Si30	1:1.2	0.852	26.58	76.73	17.38	0.85:0.15:1.2	0.870	26.90	78.04	18.27	[72]
5	PM6:BTP-eC9	PB2F	1:1.2	0.842	26.4	79.0	17.6		0.863	26.8	80.4	18.6	[73]
6	PM6:L8-BO	D18	1:1.2	0.888	25.7	79.9	18.2	0.8:0.2:1.2	0.896	26.7	81.9	19.6	[74]
7	PM6:L8-BO	D18-Cl	1:1.2	0.885	26.35	78.45	18.29	0.7:0.3:1.2	0.910	26.66	79.24	19.22	[75]
8	PM6:Y6	BR1	1:1.2	0.847	26.09	73.4	16.21	1:0.1:1.2	0.859	26.49	75.7	17.23	[77]
9	PM6:Y6	DRTB-T-C4	1:1.2	0.844	24.41	78.91	16.26	0.9:0.1:1.2	0.854	24.68	80.88	17.05	[78]
10	PM6:Y6	BTTzR	1:1.2	0.83	25.7	74.2	15.8	0.8:0.2:1.2	0.87	26.2	77.7	17.7	[79]
11	PM6:Y6	BT-CN	1:1.2	0.826	26.21	71.63	15.51	0.8:0.2:1.2	0.838	27.38	73.23	16.80	[80]
		BT-ER						0.8:0.2:1.2	0.841	27.64	74.11	17.22	
12	PM6:Y6	BTID-2F	1:1.2	0.846	25.89	75.89	16.62	0.9:0.1:1.2	0.848	27.66	76.36	17.98	[81]
13	PM6:BTP-BO-4Cl	5BDTBDD	1:1.2	0.831	25.97	74.69	16.13	0.9:0.1:1.2	0.843	26.83	77.43	17.54	[82]
14	PM6:Y6	TiC12	1:1.2	0.836	25.63	73.9	15.84	0.9:0.1:1.2	0.853	26.80	75.4	17.25	[83]

Table 4
Collections on voltage and voltage losses of ternary/quaternary organic solar cells with guest donor materials incorporated.

No.	Active layer	Guest	Binary						Ternary/quaternary						Ref.
			V_{OC} (V)	ΔE_1 (eV)	ΔE_2 (eV)	ΔE_3 (eV)	EQE_{EL} (10^{-4})	E_{loss} (eV)	V_{OC} (V)	ΔE_1 (eV)	ΔE_2 (eV)	ΔE_3 (eV)	EQE_{EL} (10^{-4})	E_{loss} (eV)	
1	PM6:Y6	PTO2	0.88	0.231	0.078	0.229	1.35	0.538	0.90	0.244	0.058	0.216	2.24	0.518	[70]
2	PM6:Y6	PM7/$PC_{71}BM$	0.842	0.236	0.066	0.256	0.505	0.564	0.848	0.247	0.065	0.255	–	0.567	[21]
									0.859	0.259	0.048	0.240	–	0.548	
3	PM6:Y6	S3	0.844	0.266	0.090	0.238	1.00	0.594	0.856	0.266	0.087	0.226	1.90	0.579	[71]
4	PM6:BTP-eC9	PM6-Si30	0.852	0.27	0.05	0.22	2.5	0.53	0.870	0.27	0.04	0.20	4.2	0.51	[72]
5	PM6:BTP-eC9	PB2F	0.842	–	–	0.231	1.3	0.559	0.863	–	–	0.218	2.2	0.531	[73]
6	PM6:L8-BO	D18	0.888	–	–	–	–	–	0.896	–	–	–	–	–	[74]
7	PM6:L8-BO	D18-Cl	0.885	0.263	0.080	0.227	1.14	0.57	0.910	0.269	0.069	0.208	2.44	0.546	[75]
8	PM6:Y6	BR1	0.847	0.268	0.055	0.229	1.4	0.552	0.859	0.262	0.048	0.224	1.7	0.534	[77]
9	PM6:Y6	DRTB-T-C4	0.844	0.230	–	0.254	0.543	0.576	0.854	0.245	0.081	0.233	1.07	0.559	[78]
10	PM6:Y6	BTTzR	0.83	0.34	–	0.23	1.4	0.58	0.87	0.34	–	0.19	5.1	0.55	[79]
11	PM6:Y6	BT-CN	0.826	0.259	0.062	0.246	0.75	0.567	0.838	0.26	0.06	0.226	1.6	0.546	[80]
		BT-ER							0.841	0.259	0.061	0.225	1.7	0.545	
12	PM6:Y6	BTID-2F	0.846	0.263	0.068	0.243	0.842	0.574	0.848	0.261	0.054	0.236	1.10	0.551	[81]
13	PM6:BTP-BO-4Cl	5BDTBDD	0.831	0.262	0.063	0.233	0.900	0.558	0.845	0.262	0.059	0.224	1.39	0.545	[82]
14	PM6:Y6	TiC12	0.836	–	0.06	0.25	–	0.58	0.853	–	0.06	0.23	–	0.55	[83]

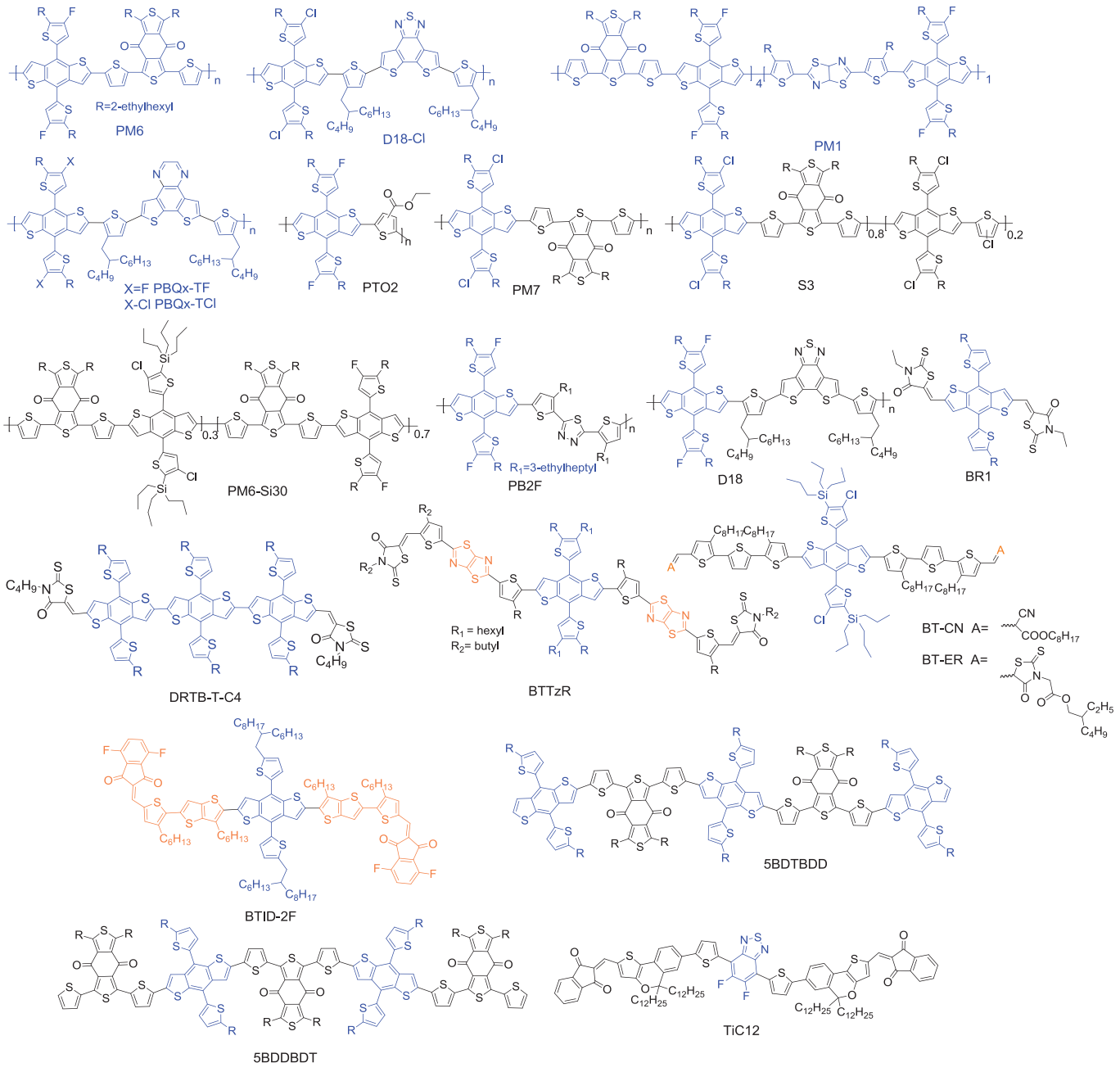

Fig. 7. Chemical structures of donors mentioned in this review.

ficient charge carrier transport and longer charge carrier lifetime, and improved phase separation sizes. The ternary devices achieved a PCE of 18.6%, a V_{OC} of 0.863 V, a J_{SC} of 26.8 mA/cm^2 and an FF of 80.4% [73].

Liu *et al.* used PM6:L8-BO as the binary system and D18 (Fig. 7) as the guest donor to construct an efficient ternary system. Both PM6 and D18 tended to form protofibril networks and a dual protofibril network morphology was formed in the PM6:L8-BO:D18 ternary blend, which effectively increased the exciton diffusion length and reduced the exciton recombination rate, facilitating exciton division and carrier generation. Studies with the density of states and the recombination mechanism using transient photocurrent, transient photovoltage and Mott-Schottky methods demonstrated that the ternary device had the lowest recombination coefficient and the highest density of states, achieved a PCE of 19.6% [74].

Huang *et al.* used D18-Cl (Fig. 7) as the guest donor of the PM6:L8-BO binary system. D18-Cl has a lower HOMO energy level compared to PM6 and the contact angle tests and DSC measurements demonstrated that the D18-Cl:PM6 formed an alloy-like donor phase. The incorporation of the guest donor reduced the HOMO-HOMO shift between donor and acceptor, reduced device non-radiative recombination losses (0.227 eV *vs.* 0.208 eV) and improved V_{OC} (0.885 V *vs.* 0.910 V). Graze-incidence wide-angle X-ray scattering (GIWAXS) showed that the ternary blended film had a larger π-π stacking peak compared to the binary blended film. The modulated phase separation facilitated charge transport and contributed to improved J_{SC} and FF. The ternary device gave an efficiency of 19.22% [75].

The deep-HOMO-level guest donor constructed on the basis of the BDT unit has a similar structure with the current star molecule PM6, thus ensuring good miscibility, the formation of an alloy-like

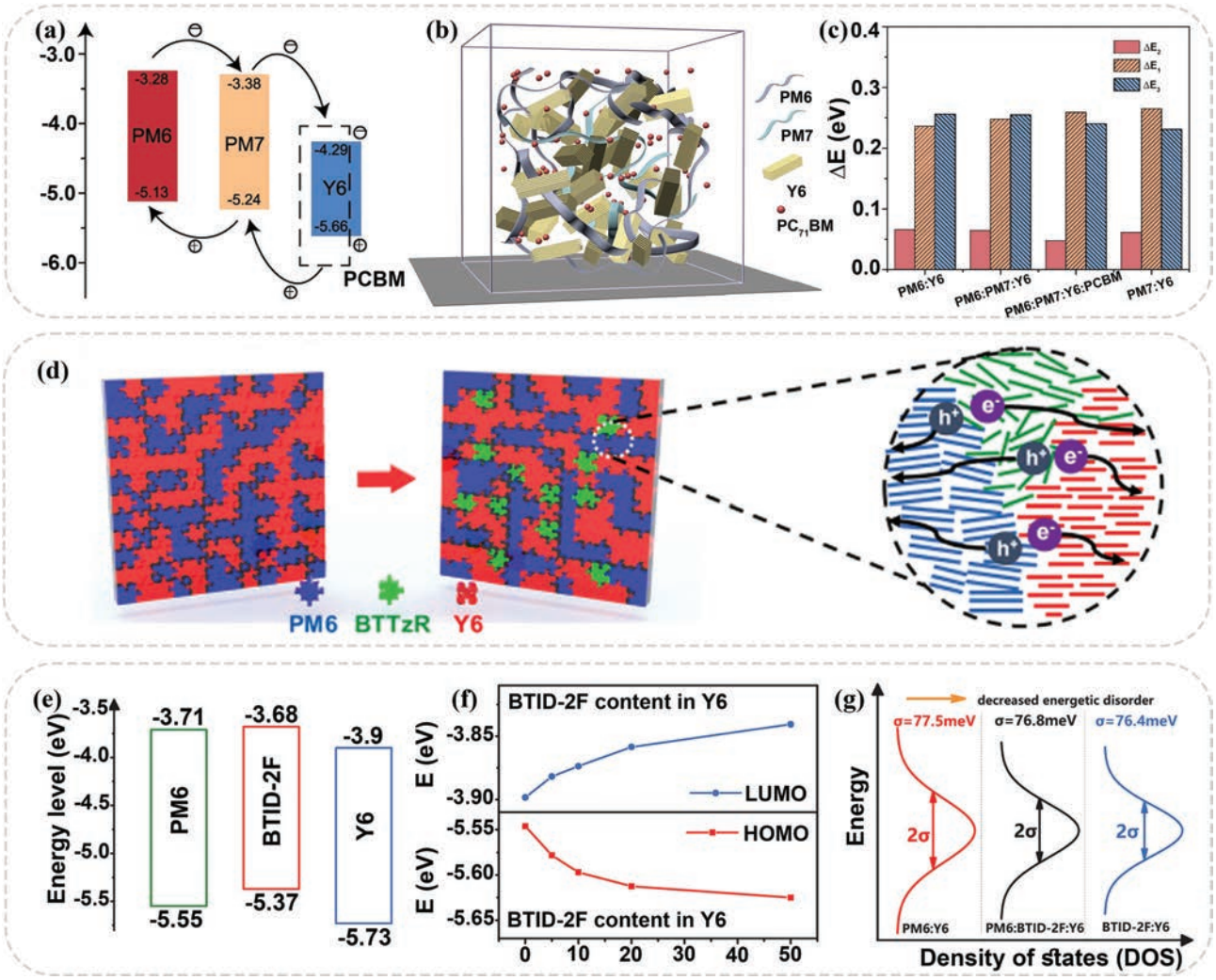

Fig. 8. (a) Energy level alignment and double cascading transport pathways for quaternary system. (b) The arrangement sketch of molecules in quaternary blended films. (c) Energy loss histogram, including ΔE_1, ΔE_2, and ΔE_3 of blended devices. Copied with permission [21]. Copyright 2021, Nature Publishing Group. (d) Visual illustration of the phase distribution in binary and ternary blend films, the blue, green and red puzzle blocks and rods represent PM6, BTTzR and Y6, respectively. Copied with permission [79]. Copyright 2021, Elsevier Publication Group. (e) Schematic energy diagrams of PM6, BTID-2F, and Y6. (f) Energy levels of blend films dependence on BTID-2F weight ratios. (g) Schematic illustration of the impact of binary and optimized ternary devices on the electron transport and energetic disorder. Copied with permission [81]. Copyright 2022, Wiley Publishing Group.

phase and optimized morphology. Also, the formation of the alloy phase can pull down its overall HOMO energy level as well as reduce the HOMO-HOMO energy offset between D-A, which is beneficial to the reduction in the non-radiative recombination loss of the device and the improvement in the open-circuit voltage.

4.2. Crystallinity

The shape of the active layer has a significant impact on the performance of OSCs. The formation of a suitable scale of phase separation and a bi-continuous structure is essential for the improvement of efficiency and stability, and crystallization is an important way to regulate the shape of the active layer. Small-molecule donor is usually highly crystalline and it can be used in the construction of high-performance ternary system to effectively improve the crystallinity of the blended film, which helps to regulate the crystallinity of the donor and to optimize the active layer morphology, thus to improve the performance and stability of the device [76].

Wu *et al.* introduced A-D-A type small-molecule donor, BR1 (Fig. 7), with BDT as the central unit and rhodanine as the end group, into the PM6:Y6 blends. The calculated ω value of 1.49 for the ternary blended film was greater than 1, indicating that BR1 was selectively dispersed into the donor phase. The addition of 10 wt% of BR1 modulated molecular stacking and aggregation in the blended film, increased the CCL (11.3 Å *vs.* 18.8 Å), formed tighter π-π stacking (3.61 Å *vs.* 3.57 Å), reduced bimolecular recombination, hence enhanced J_{SC} and FF. ΔE_2 was reduced from 0.055 eV to 0.048 eV and ΔE_3 from 0.229 eV to 0.224 eV for the ternary devices compared to the binary devices, gaining 17.23% efficiency [77].

Bao *et al.* reported a highly crystalline small-molecule donor (DRTB-T-C4) (Fig. 7) by coupling three BDT-cores, *e.g.,* electron-rich units with two rhodanine-terminated groups, which was incorporated into the PM6:Y6 binary system to form a highly ordered structure with morphology optimized, hence resulting in improved hole and electron mobility and a more balanced μ_h/μ_e. A series of transient characterization techniques demonstrated faster exciton dissociation, more efficient charge carrier generation and suppressed charge recombination, resulted in 80.88% FF. The introduction of the guest donor improved the EQE_{EL} (1.07×10^{-4} *vs.* 5.43×10^{-5}) and reduced energetic disorder (E_U: 23.6 meV *vs.* 26.1 meV) achieved a V_{OC} enhancement, achieved a PCE of 17.05%. [78].

Li *et al*. used the small-molecule donor BTTzR (Fig. 7), which has strong crystalline properties, as a guest donor adding into the PM6:Y6 binary system. When 20 wt% of BTTzR was added, the CCL of PM6 increased from 9.78 Å to 9.82 Å and the CCL of Y6 increased from 26.06 Å to 27.45 Å The introduction of the guest donor enhanced the crystallinity and phase purity of the binary blended film, reduced the aggregation of Y6, suppressed charge carrier recombination, promoted carrier transport and improved FF. The 0.8:0.2:1.2 blended PM6:BTTzR:Y6 obtained better phase separation, reduced non-radiative recombination losses (0.23 eV *vs*. 0.19 eV), achieved a significant increase in V_{OC} from 0.83 V to 0.87 V and obtained a PCE of 17.7% (Fig. 8d) [79].

Wang *et al*. synthesized BT-CN and BT-ER (Fig. 7) by replacing BDT with 4,8-bis(4–chloro-5-(tripropylsilyl)thiophen-2-yl)benzo[1,2-*b*:4,5-*b*']dithiophene (BDTT-SiCl) as the core and combined it with end-group engineering. When blending 20 wt% of BT-CN and BT-ER with PM6:Y6, respectively, the ternary blended films showed higher crystallinity (CCL: 23.97 Å *vs*. 25.74 Å and 27.91 Å) and more ordered orientation, which facilitated charge dissociation and transport and increased J_{SC} and FF. Meanwhile, the ternary devices showed enhanced EQE_{EL} (0.75×10^{-4} *vs*. 1.6×10^{-4} and 1.7×10^{-4}) with reduced E_{loss} of 0.546 eV and 0.545 eV for PM6:BT-CN:Y6 and PM6:BT-ER:Y6, respectively, which was in line with the V_{OC} variations of the corresponding devices. The ternary devices achieved 16.80% PCE (V_{OC} of 0.838 V, J_{SC} of 27.38 mA/cm^2 and FF of 73.23%) and 17.22% PCE (V_{OC} of 0.841 V, J_{SC} of 27.64 mA/cm^2 and FF of 74.11%), respectively. Used BT-CN and BT-ER as guest donor for PM6:L8-BO, 18.05% and 18.11% efficiencies were achieved, respectively [80].

4.3. Energetic disorder tuning

Apart from selecting guest donor with lower HOMO energy levels, some studies have shown that guest donor with redshift band gap can also achieve both V_{OC} and J_{SC} improvement. Wei *et al*. have introduced BTID-2F (Fig. 7), a small-molecule donor with a narrower band gap than PM6, into the PM6:Y6 binary system. BTID-2F (−5.37 eV) had a higher HOMO energy level compared to PM6 (−5.55 eV), and the red-shift of the external quantum efficiency indicated that the ternary co-blend have a narrower band gap and better aggregation. It was interesting to note that as the ratio of guest donor increased, the energy offset between the HOMO energy level of the co-blended donor and the LUMO energy level of the co-blended acceptor increased with the ternary device exhibiting reduced energy disorder and reduced energy loss, achieving a V_{OC} improvement. Addition of BTID-2F resulted in the formation of tighter π-π stacking in the blended film and enhanced crystallinity, which promoted charge transport and suppressed molecular recombination with simultaneous improvement of J_{SC} and FF. The ternary device achieved a PCE of 17.98% (Figs. 8e-g). As well, the substitution of the Y6 acceptor with the L8-BO molecule further increased the PCE to 18.52%, demonstrating its generality [81]. Li *et al*. synthesized two A-D-A-D-A and D-A-D-A-D type oligomers, 5BDTBDD and 5DDBDT (Fig. 7), by alternating coupling of BDT and BDD units. 5BDTBDD and 5DDBDT had up-shifted HOMO/LUMO energy levels (−3.53/−5.40 eV, −3.58/−5.27 eV *vs*. −3.59/−5.48 eV) and a red-shifted band gap (1.86/1.83 eV *vs*. 1.81 eV), which were, respectively, added as guest donors to the PM6:BTP-BO-4Cl binary system. Contact angle measurements indicated good miscibility of the oligomer 5BDTBDD with BTP-BO-4Cl, significantly reduced the aggregation-induced emission quenching effect. Therefore, based on PM6:5BDTBDD:BTP-BO-4Cl (0.9:0.1:1.2) the ternary device (23.9 meV) showed a smaller E_U than the PM6:BTP-BO-4Cl binary device (26.4 meV), indicating a reduced energetic disorder in the ternary blends. The ternary device exhibited a higher EQE_{EL} value, an effectively reduced ΔE_3 value (0.233 eV *vs*. 0.224 eV) and an improved V_{OC}. The larger electrostatic potential (ESP) between 5BDTBDD or 5BDDBDT and BTP-BO-4Cl promoted the dissociation of excitons. Upon treatment with *o*-xylene as a green solvent, the BDTBDD-based ternary devices exhibited a PCE of 17.54% [82].

Besides the BDT unit, other excellent units such as BT, IDT are also available for designing donor molecules. Zhu *et al*. introduced a small molecule donor, *e.g.,* TiC12 (Fig. 7) with a symmetric thieno[3,2-*c*]isochromene units into the PM6:Y6 system. TiC12 (−5.45 eV) exhibited a higher HOMO energy level than PM6 (−5.56 eV) and showed good miscibility with Y6. Compared to PM6:Y6, the ternary device containing 10 wt% of TiC12 showed a smaller energetic disorder value (65 meV *vs*. 63 meV). The incorporation of the guest enhanced the crystallinity of the blended film (CCL: 21.6 Å *vs*. 23.0 Å), ensured effective charge transfer in the vertical direction, and reduced the non-radiative energy loss (0.25 eV *vs*. 0.23 eV). The device performance achieved simultaneous improvement in V_{OC} (0.836 V *vs*. 0.853 V), J_{SC} (25.63 mA/cm^2 *vs*. 26.80 mA/cm^2), and FF (73.9% *vs*. 75.4%). The ternary device based on M6:TiC12:Y6 (0.9:0.1:1.2) achieved an efficiency of 17.25% [83].

These works demonstrate that V_{OC} is not exclusively determined by lower HOMO. By introducing conjugated small molecules or oligomers with unfavorable energy arrangements, upshifted HOMO levels can also contribute significantly to V_{OC} enhancement if a balanced DOS is obtained. It is also a novel strategy for the preparation of high performance OSCs, a strategy that offers the possibility of a wider choice of third components and a new idea for constructing ternary OSCs with improved PCEs.

5. Conclusions and outlook

In summary, the ternary-quaternary strategy is an effective way to reduce voltage losses, which can be achieved in several ways: (1) By incorporating guest materials to achieve modulation of the miscibility of the blended film, to optimize the morphology, to modulate the phase separation scale, to enhance or inhibit the aggregation of the host acceptors, to reduce their self-quenching, and thus to reduce non-radiative recombination; (2) Combining molecular design strategies (asymmetric design, halogenation on end-group, *etc.*) to design and synthesize materials with high photoluminescence quantum efficiency as guest components to enhance electroluminescence and reduce radiative and non-radiative recombination losses; (3) Through the addition of guest materials, the crystallinity of the blended film can be adjusted to optimize the morphology, to suppress energetic disorder in the blended film, to reduce charge carrier, to reduce voltage loss and to increase open-circuit voltage. Meanwhile, the introduction of guests can effectively improve the charge transport properties of the blended film, promote charge extraction and increase the short-circuit current density and fill-factor. The ultimate performance improvement is achieved.

Currently, OSCs are on the point of stepping up to 20% efficiency and the ternary/quaternary strategy has been proven by many efforts effective means of further improving device performance. The next steps for ternary-quaternary OSCs should be to develop them in the following ways:

(1) Reducing voltage loss through modulation on acceptor ESP: In OSC devices, the degree of CT at the donor/acceptor interface is related to the intermolecular interactions [84]. It has been shown that enhanced intermolecular interactions will increase the CT state ratio when they hybridize with the LE state, which can promote charge generation, and also can lead to large non-radiative recombination loss. Till now, there yet no well-defined molecular design strategies for designing photovoltaic materials with suppressed non-radiative recombination loss in OSCs. From a chemical structure point

of view, intermolecular interactions are related to the ESP distribution on the molecular surface [85]. By tuning the ESP distribution of the given acceptor material to achieve a balance between the CT and LE states in the device, the tuning of the device voltage loss can be achieved and the device PCE can be further enhanced [86].

(2) Developing high luminescent guest components: The incorporation of high luminescent guest materials can help to achieve a reduced voltage loss and a range of materials with high luminescence should be further developed from a molecular design perspective.

(3) Understanding the underlying mechanisms: The incorporation of guest materials has achieved impressive structures in terms of device efficiency and stability, but it is not just a simple addition in terms of components, the complexity of the intrinsic working mechanism is much higher than that of the binary devices, and the working mechanism of how the guest materials function in the main material is still not very clear in the present study and needs to be further explored systematically in terms of phase structure and energy changes.

(4) Seeking thick-film material system: The development of highly efficient ternary/quaternary systems for thick film or large-area devices, setting the stage for future commercialization of OSCs.

(5) Seeking processing methods: Simple variations in the fabrication process often lead to further improvements in performance, such as layer-by-layer spin coating. The development of simple and effective fabrication processes combined with a ternary/quaternary strategy is also essential for efficiency improvements.

Declaration of competing interest

The authors declare that they have no conflict of interest.

Acknowledgments

The authors acknowledge the financial supports from the Department of Science and Technology of Inner Mongolia (No. 2020GG0192), the Natural Science Foundation of Inner Mongolia (No. 2022ZD04), the Inner Mongolia Normal University (No. 112/1004031962), and the Inner Mongolia Autonomous Region Postgraduate Research Innovation Fund (No. S20210274Z).

References

[1] K. Chong, X. Xu, H. Meng, et al., Adv. Mater. 34 (2022) 2109516.
[2] Y. Wei, Z. Chen, G. Lu, et al., Adv. Mater. 34 (2022) 2204718.
[3] Q. Liu, Y. Jiang, K. Jin, et al., Sci. Bull. 65 (2020) 272–275.
[4] D. Qian, L. Ye, M. Zhang, et al., Macromolecules 45 (2012) 9611–9617.
[5] C. Sun, F. Pan, H. Bin, et al., Nat. Commun. 9 (2018) 743.
[6] A. Zeng, X. Ma, M. Pan, et al., Adv. Funct. Mater. 31 (2021) 2102413.
[7] M. Zhang, X. Guo, W. Ma, H. Ade, J. Hou, Adv. Mater. 27 (2015) 4655–4660.
[8] Z. Zheng, H. Yao, L. Ye, et al., Mater. Today 35 (2020) 115–130.
[9] X. Zhang, Z. Lu, L. Ye, et al., Adv. Mater. 25 (2013) 5791–5797.
[10] Y. Lin, J. Wang, Z. Zhang, et al., Adv. Mater. 27 (2015) 1170–1174.
[11] J. Yuan, Y. Zhang, L. Zhou, et al., Joule 3 (2019) 1140–1151.
[12] K. Li, Y. Wu, Y. Tang, et al., Adv. Energy Mater. 9 (2019) 1901728.
[13] A. Pan, T. Lau, Y. Tang, et al., J. Mater. Chem. A 7 (2019) 20713–20722.
[14] Y. Chang, T. Lau, M. Pan, et al., Mater. Horizon. 6 (2019) 2094–2102.
[15] Y. Chang, T.K. Lau, P.Y. Chow, et al., J. Mater. Chem. A 8 (2020) 3676–3685.
[16] W. Zhang, H. Huang, J. Xu, et al., Adv. Energy Mater. 10 (2020) 2001436.
[17] H. Tan, W. Zhang, P. Zhang, et al., Solar RRL 6 (2022) 2200147.
[18] W. Zhang, J. Huang, X. Lv, et al., Chin. Chem. Lett. 34 (2023) 107436.
[19] Z. Wang, Y. Zhang, J. Zhang, Z. Wei, W. Ma, Adv. Energy Mater. 6 (2016) 1502456.
[20] W. Li, D. Yan, F. Liu, et al., Sci. China Chem. 61 (2018) 1609–1618.
[21] M. Zhang, L. Zhu, G. Zhou, et al., Nat. Commun. 12 (2021) 309.
[22] F. Zhao, H. Zhang, R. Zhang, et al., Adv. Energy Mater. 10 (2020) 2002746.
[23] S.D. Stranks, R.L.Z. Hoye, D. Di, R.H. Friend, F. Deschler, Adv. Mater. 31 (2019) 1803336.
[24] J. Yuan, H. Zhang, R. Zhang, et al., Chem 6 (2020) 2147–2161.
[25] H. Yao, J. Hou, Angew. Chem. Int. Ed. 61 (2022) 202209021.
[26] J. Gao, W. Gao, X. Ma, et al., Energy Environ. Sci. 13 (2020) 958–967.
[27] B.A. Collins, Z. Li, C.R. McNeill, H. Ade, Macromolecules 44 (2011) 9747–9751.
[28] Q. Zhao, Z. Xiao, J. Qu, et al., ACS Energy Lett. 4 (2019) 1106–1114.
[29] H. Naveed, W. Ma, Joule 2 (2018) 621–641.
[30] S. Honda, H. Ohkita, H. Benten, S. Ito, Adv. Energy Mater. 1 (2011) 588–598.
[31] W. Yang, W. Wang, Y. Wang, et al., Joule 5 (2021) 1209–1230.
[32] H. Tan, B. Yuan, Z. Shao, et al., Chem. Eng. J. 445 (2022) 136691.
[33] S. Dai, M. Li, J. Xin, et al., J. Mater. Chem. A 10 (2022) 1948–1955.
[34] M. Jiang, H. Zhi, B. Zhang, et al., ACS Energy Lett. 8 (2023) 1058–1067.
[35] F. Liu, L. Zhou, W. Liu, et al., Adv. Mater. 33 (2021) 2100830.
[36] X. Ma, A. Zeng, J. Gao, et al., Natl. Sci. Rev. 8 (2021) 305.
[37] L. Ye, S. Li, X. Liu, et al., Joule 3 (2019) 443–458.
[38] Z. Bi, H. Naveed, H. Wu, et al., Adv. Energy Mater. 12 (2022) 2103735.
[39] L. Zhan, S. Li, T.K. Lau, et al., Energy Environ. Sci. 13 (2020) 635–645.
[40] X. Yan, J. Wu, J. Lv, et al., J. Mater. Chem. A 10 (2022) 15605–15613.
[41] Y. Li, Y. Cai, Y. Xie, et al., Energy Environ. Sci. 14 (2021) 5009–5016.
[42] Y. Cai, Y. Li, R. Wang, et al., Adv. Mater. 33 (2021) 2101733.
[43] F.D. Eisner, M. Azzouzi, Z. Fei, et al., J. Am. Chem. Soc. 141 (2019) 6362–6374.
[44] S. Li, L. Zhan, Y. Li, et al., Small Methods 6 (2022) 2200828.
[45] Y. Cui, H. Yao, J. Zhang, et al., Nat. Commun. 10 (2019) 2515.
[46] J. Guo, Z. Zhang, T. Guan, et al., Chem. Sci. 10 (2019) 8792–8798.
[47] J. Yuan, C. Zhang, H. Chen, et al., Sci. China Chem. 63 (2020) 1159–1168.
[48] S. Liu, J. Yuan, W. Deng, et al., Nat. Photonics 14 (2020) 300–305.
[49] W. Liu, J. Zhang, S. Xu, X. Zhu, Sci. Bull. 64 (2019) 1144–1147.
[50] Z.P. Yu, X. Li, C. He, et al., Chin. Chem. Lett. 31 (2020) 1991–1996.
[51] J. Wan, I. Dyadishchev, R. Sun, et al., J. Mater. Chem. A 10 (2022) 17122–17131.
[52] W. Liu, S. Sun, L. Zhou, et al., Angew. Chem. Int. Ed. 61 (2022) 202116111.
[53] P. Bi, S. Zhang, Z. Chen, et al., Joule 5 (2021) 2408–2419.
[54] H. Lu, W. Liu, H. Jin, et al., Adv. Funct. Mater. 32 (2021) 2107756.
[55] A. Lan, Y. Lv, J. Zhu, et al., ACS Energy Lett. 7 (2022) 2845–2855.
[56] Y. Xu, Y. Cui, H. Yao, et al., Adv. Mater. 33 (2021) 2101090.
[57] Y. Cui, Y. Xu, H. Yao, et al., Adv. Mater. 33 (2021) 2102420.
[58] C. He, Y. Pan, Y. Ouyang, et al., Energy Environ. Sci. 15 (2022) 2537–2544.
[59] S. Li, L. Zhan, Y. Jin, et al., Adv. Mater. 32 (2020) 2001160.
[60] C. He, Z.Z. Chen, T. Wang, et al., Nat. Commun. 13 (2022) 2598.
[61] R. Sun, Y. Wu, X. Yang, et al., Adv. Mater. 34 (2022) 2110147.
[62] N. Kazerouni M. Günther, T. Ameri, Nat. Rev. Mater. 8 (2023) 456–471.
[63] S. Xie, Y. Xia, Z. Zheng, et al., Adv. Funct. Mater. 28 (2018) 1705659.
[64] T. Zhang, Y. Xu, H. Yao, et al., Energy Environ. Sci. 16 (2023) 1581–1589.
[65] H. Chen, Y. Zou, H. Liang, et al., Sci. China Chem. 65 (2022) 1362–1373.
[66] L. Zhan, S. Li, Y. Li, et al., Joule 6 (2022) 662–675.
[67] L. Zhan, S. Li, Y. Li, et al., Adv. Energy Mater. 12 (2022) 2201076.
[68] L. Zhan, S. Yin, Y. Li, et al., Adv. Mater. 34 (2022) 2206269.
[69] R. Zhou, Z. Jiang, C. Yang, et al., Nat. Commun. 10 (2019) 5393.
[70] B. Jiang, Y. Peng, Y. Su, et al., Chem. Eng. J. 431 (2022) 133950.
[71] Q. An, J. Wang, X. Ma, et al., Energy Environ. Sci. 13 (2020) 5039–5047.
[72] W. Peng, Y. Lin, S.Y. Jeong, et al., Nano Energy 92 (2022) 106681.
[73] T. Zhang, C. An, P. Bi, et al., Adv. Energy Mater. 11 (2021) 2101705.
[74] L. Zhu, M. Zhang, J. Xu, et al., Nat. Mater. 21 (2022) 656–663.
[75] J. Gao, N. Yu, Z. Chen, et al., Adv. Sci. 9 (2022) 2203606.
[76] K. Sun, Z. Xiao, S. Lu, et al., Nat. Commun. 6 (2015) 6013.
[77] H. Feng, Y. Dai, L. Guo, et al., Nano Res. 15 (2021) 3222–3229.
[78] Y. Zeng, D. Li, Z. Xiao, et al., Adv. Energy Mater. 11 (2021) 2101338.
[79] Q. Liu, Y. Wang, J. Fang, et al., Nano Energy 85 (2021) 105963.
[80] J. Li, C. Zhang, X. Zhong, et al., Small 19 (2023) 2205572.
[81] Y. Yan, Y. Zhang, Y. Liu, et al., Adv. Energy Mater. 12 (2022) 2200129.
[82] H. Xia, Y. Zhang, W. Deng, et al., Adv. Mater. 34 (2022) 2107659.
[83] W. Tang, W. Peng, M. Zhu, et al., J. Mater. Chem. A 9 (2021) 20493–20501.
[84] Q. Liu, K. Vandewal, Adv. Mater. 35 (2023) 2302452.
[85] Y. Xu, H. Yao, L. Ma, et al., Angew. Chem. Int. Ed. 59 (2020) 9004–9010.
[86] L. Ma, H. Yao, J. Zhang, et al., Chem 9 (2023) 1–12.